MEASUREMENT AND INTERPRETATION OF CRUSTAL DEFORMATION RATES ASSOCIATED WITH POSTGLACIAL REBOUND

GRANT NAG5-1930

Semiannual Status Report No. 5

For the Period 14 March 1994 through 15 September 1994

Principal Investigator

Dr. James L. Davis

October 1994

Prepared for

National Aeronautics and Space Administration
Washington, D.C. 20546

Smithsonian Institution
Astrophysical Observatory
Cambridge, Massachusetts 02138

The Smithsonian Astrophysical Observatory is a member of the Harvard-Smithsonian Center for Astrophysics

The NASA Technical Officer for this Grant is Dr. Bruce Bills, Code 921, Laboratory for Terrestrial Physics, Earth Sciences Directorate, NASA Goddard Space Flight Center, Greenbelt, Maryland 20771

I. Introduction

This project involves obtaining GPS measurements in Scandinavia, and using the measurements to estimate the viscosity profile of the Earth's mantle and to correct tide-gauge measurements for the rebound effect. Below, we report on several aspects of this project.

II. GPS Measurements

The permanent network set up by Onsala Space Observatory continues to operate, and the data are continuously being analyzed. The expanded DSGS was occupied during the latter half of August, 1994. The expanded DSGS included a number of tide-gauge sites in Sweden and Finland.

III. Error Sources

We have performed an extensive investigation of the influence of signal scattering on the estimates of site position. In this investigation, we have determined that signal scattering (i.e., reflections in the near field) associated with the pillar for permanent GPS setups have a large influence on these estimates. We have prepared a manuscript for submission to *J. Geophys. Res.*, and included this manuscript in the Appendix.

IV. Analysis of Tide-gauge Data

We have used the Baltic Sea sea-level record to estimate site-referenced sea-level rates, i.e., sea-level rates referenced to one site. These estimates are not influenced by any common sea-level changes, which may be associated with, e.g., global change. We have compared these estimates to predictions of site-referenced sea-level rates determined using the formalism of *Mitrovica et al.* [1994a] and calculated χ^2 differences. These differences are shown in Figure 1. These differences clearly show a preference for weak upper-mantle viscosities and thinner lithospheres. These results are in agreement with the results of *Mitrovica et al.* [1994b], which were obtained using VLBI data only.

References

Mitrovica, J.X., J.L. Davis, and I.I. Shapiro, A spectral formalism for computing three-dimensional deformations due to surface loads, 1. Theory, *J. Geophys. Res.*, in press, 1994a.

Mitrovica, J.X., J.L. Davis, and I.I. Shapiro, A spectral formalism for computing three-dimensional deformations due to surface loads, 2. Present-day glacial isostatic adjustment, *J. Geophys. Res.*, in press, 1994b.

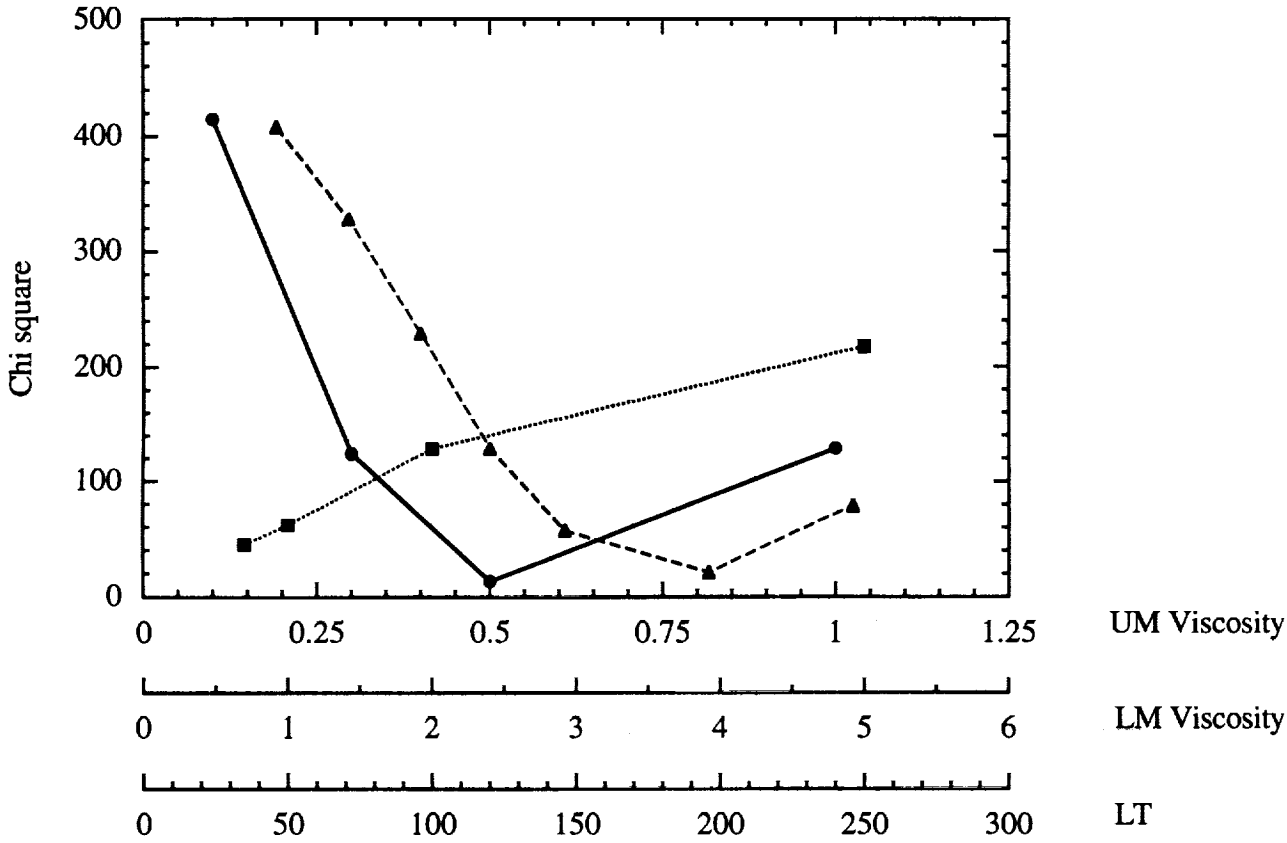

Figure 1. Values of chi-squared differences between the site-referenced sea-level rates determined from tide-gauge data and from model calculations. The standard Earth model used for the calculations had a lithospheric thickness of 120 km, an upper mantle viscosity of 10**21 Pa s, and a lower mantle viscosity of 2 x 10**21 Pa s. Each of the curves above represents the valriation ofthe values of each of these parameters: Lithospheric thickness (dasehd), upper mantle (solid), and lower mantle (dotted). The scales for the viscosity values are scalings of 10**21 Pa s, and that for the lithospheric thickness is km.

Appendix. Elósegui et al., in preparation

Geodesy using the Global Positioning System: The effects of signal scattering on estimates of site position

P. Elósegui[1], J. L. Davis[1], R. T. K. Jaldehag[2], J. M. Johansson[2] A. E. Niell[3], and I. I. Shapiro[1]

[1]Harvard-Smithsonian Center for Astrophysics, Cambridge, Massachusetts
[2]Onsala Space Observatory, Chalmers University of Technology, Onsala, Sweden
[3]Haystack Observatory, Massachusetts Institute of Technology, Westford, Massachusetts

Received _____; accepted _____

Short title: EFFECTS OF SCATTERING ON GPS GEODESY

Abstract.

Analysis of Global Positioning System (GPS) data from two sites separated by a horizontal distance of only ~2.2 m yielded phase residuals exhibiting a systematic elevation angle dependence. One of the two GPS antennas was mounted on an ~1 m high concrete pillar, and the other was mounted on a standard wooden tripod. We performed elevation angle cutoff tests with these data, and established that the vertical coordinate of site position was sensitive to the minimum elevation angle (elevation cutoff) of the data analyzed. For example, the vertical coordinate of site position changed by 9.7±0.8 mm when the minimum elevation angle was increased from 10° to 25°. We performed simulations based on a simple (ray tracing) multipath model with a single horizontal reflector, and demonstrated that the elevation angle cutoff test results and the pattern of the residuals versus elevation angle could be qualitatively reproduced if the reflector were located 0.1–0.2 m beneath the antenna phase center. We therefore hypothesized that the source of the elevation-angle-dependent error were multipath reflections and scattering and that the horizontal surface of the pillar, located a distance of ~0.2 m beneath the antenna phase center, was the primary reflector. We tested this hypothesis by placing microwave absorbing material between the antenna and the pillar in a number of configurations and analyzed the changes in apparent position of the antenna. The results indicate that (1) the horizontal surface of the pillar is indeed the main reflector, (2) both the concrete and the metal plate embedded in the pillar are significant reflectors, and (3) the reflections can be reduced to a great degree by the use of microwave absorbing materials. These results have significant implications for the accuracy of global GPS geodetic tracking networks which use pillar-antenna configurations identical or similar to the one used here (at the Westford WFRD GPS site).

Introduction

Surveying with the NAVSTAR Global Positioning System (GPS) is a technique of increasingly widespread utility in civil and scientific applications requiring position, velocity, and acceleration determinations and time synchronization. First put into widespread use in the mid-1980's, GPS is the latest of the so-called space geodetic techniques and can already compete in accuracy with other existing techniques at all terrestrial spatial scales (station separation $\leq$ 12,000 km), including Very-Long-Baseline Interferometry (VLBI) and Satellite Laser Ranging (SLR). The demonstrated repeatability of horizontal position estimates obtained from GPS data is currently at the 1–2 mm level on local and regional scales ($\leq$ 500 km), and it is approaching, if it has not obtained, the 10 mm level on global scales [e.g., Dixon, 1991; Blewitt, 1993]. Typical values for vertical baseline component repeatability are a factor of 3–5 greater. This gain in repeatability has been obtained by the improvement of the satellite constellation and by the establishment of global permanent GPS networks for continuous satellite tracking and orbit determination. These advances have triggered the introduction around the world of continuously operating GPS arrays on local, regional, and global scales, for studying a wide range of geophysical phenomena.

The Global Positioning System consists of a constellation of 26 satellites plus three active spares in nearly circular orbits, distributed in six distinct orbital planes each having an inclination close to 55° (several have inclinations closer to 62°). The orbital radii of the satellites are ~26,000 km, giving them a period of 12 hours, so that the configuration relative to the Earth repeats itself once every sidereal day. Each GPS satellite transmits highly coherent radio signals with right-hand circularl polarization (RCP) over two L-band channels, L1 (1575.42 GHz) and L2 (1227.60 GHz). Each of these L-band carrier signals is modulated by two pseudo-random noise (PRN) sequences, called the precision (P) code (10.23 MHz) and the coarse/acquisition (C/A) code (1.023 MHz), the latter on L1 only. The three signals are modulated, in

turn, by a 50 Hz data stream which transmits the satellite's ephemeris and health, clock-biases, ionospheric propagation correction data, and other useful information. All of the transmitted signals are governed by a combination of four onboard atomic clocks. Geodetic GPS receivers are capable of observing eight to twelve GPS satellites simultaneously. Additional details concerning the Global Positioning System can be found in Dixon [1991] and Blewitt [1993] and references therein.

There are two main GPS observation types: the pseudo-range (P-code) and the carrier beat phase observations. The statistical error of the latter is about 100-fold smaller than that of the former. For geodetic positioning applications, therefore, the basic observable is the carrier beat phase, which is the difference between the phase of the signal received by the ground-based GPS antenna/receiver system from a given satellite and a signal of the appropriate frequency generated by the internal oscillator of the GPS receiver. The carrier beat phase is determined independently for each channel, L1 and L2. The carrier beat phase observable ϕ_i for the ith frequency channel (i.e., $i = 1$ for L1 and $i = 2$ for L2) can thus be expressed (in cycles), at some epoch t, [e.g., King et al., 1985] as

$$\phi_i = \frac{\rho}{\lambda_i} + C_i^{\mathrm{rec}} - C_i^{\mathrm{sat}} + \phi^{\mathrm{atm}} - \phi_i^{\mathrm{ion}} - \phi_i^{\mathrm{apr}} + N + \epsilon_i \qquad (1)$$

where ρ is the instantaneous distance between the receiving antenna and satellite, λ_i is the wavelength associated with the ith channel, C_i^{rec} is the receiver "clock" phase error due mainly to drifting of the receiver frequency standard from the nominal frequency, C_i^{sat} is the satellite "clock" phase error due to the same problem in the transmitting satellite, ϕ^{atm} is the phase delay due to the neutral atmosphere (nondispersive up to frequencies close to 60 GHz; see, e.g., Liebe [1985]), ϕ_i^{ion} is the dispersive ionospheric phase delay, ϕ^{apr} is the a priori phase delay or difference between the initial phases of the satellite and the receiver, N is an integer cycle bias or "ambiguity," and ϵ_i is the phase measurement error, random and otherwise, due to other sources (see below). The

less precise pseudo-range code observation equation, on the other hand, is comparable to that of the carrier beat phase except for the initial cycle ambiguity term and for the sign of the ionospheric term.

The satellite and receiver "clock" errors are easily and accurately dealt with using the method of double differencing, or its equivalent (e.g., Counselman and Shapiro, 1979; Wells et al., 1986), which uses between-station and between-satellite differences to estimate these quantities. The ionospheric phase delay is estimated by combining the carrier beat phase observables from the two frequencies [e.g., Spilker, 1978]. Such a combined observable will here be referred to as the "linear combination", or "LC", observable. The LC observations from multiple sites, satellites, and epochs are combined to estimate a number of parameters, including the integer ambiguities for all the site/satellite combinations, zenith atmospheric propagation delays, site positions, satellite orbital parameters, and other relevant parameters.

The main goal of this work is to study the effects of carrier-phase signal scattering on geodetic estimates of site position obtained from GPS data. Signals scattered or reflected off objects in the environment of the GPS antenna will interfere with the unreflected signal. (A signal can be both reflected and scattered.) Thus, reflections will contribute to the measured phase to an extent which depends on the lengths of the paths travelled by the unreflected and reflected signals from their origin to the receiving antenna. Both the carrier phase and the pseudo-range coded signals can suffer, though differently, from these effects. In general, the estimates of positions obtained from reflection-contaminated GPS carrier-phase and/or pseudo-range observations will be in error.

The term multipath is used in the GPS literature to refer to the reflected signal. It is implicit in this effect that the reflecting structure is located in the far-field of the antenna. In this zone, the shape of the antenna field pattern is independent of the distance, and therefore its electromagnetic properties are not affected by the presence of

reflectors. Geometrical ray optics is appropiate to describe the multipath effect. On the other hand, when the reflecting structure (or any conducting material) is placed in the near-field of the antenna, there occurs a coupling of these elements with the antenna and its electromagnetic properties will change because, in general, the shape of the antenna field pattern dependens on the distance. Difraction and scattering effects from the edges of the antenna and off the reflecting structures within this zone may be of significant contribution, and physical optics should be used to describe these effects. The coupling in the near-field makes important to characterize the electrical properties of the GPS antenna used for geodetic measurements not only in e.g., an anechoic chamber but also as they may appear in field operation.

The effects of transmitting and receiving element multipath interference on the code and on the phase GPS observables have been addressed at some depth in the GPS literature. Counselman and Gourevitch [1981] studied the effects of multipath interference and sky blockage on a method of ambiguity resolution. Young et al. [1985] experimented with multipath effects originating at the Block I GPS satellite antenna and derived an expression for the error on the pseudo-range and carrier-signal observables introduced by single multipath reflections. This effect will be the same at all receiving antennas for sites located close together and will therefore cancel out in difference positioning involving close sites. Although we have not addressed the effect in this paper, similar efforts to assess quantitatively the impact of multipath caused by the Block II satellites on global positioning should be carried out, especially as the accuracy of geodetic measurements with GPS improves. Many tests have been performed to evaluate the severity of the signal multipath effects on the GPS pseudo-range measurements [Bletzacker, 1985] and its impact on the accuracy of orbit determinations [Evans and Carr, 1989]. Many tests also have dealt with inducing such errors by means of artificial reflectors placed near the antenna to study the effect in controlled environments [e.g., Greenspan et al., 1982; Tranquilla, 1986; Tranquilla et

al., 1986]. Georgiadou and Kleusberg [1988] discussed errors in GPS carrier beat phase observables resulting from multipath interference and presented a mathematical model for multipath errors produced by multiple simultaneous reflections.

The multipath as a potential source of error on geodetic estimates of site position from GPS data has been discussed in some detail in the literature. Davis et al. [1989] found the effect of multipath on ~20 m baselines to be limited to ~1 mm both in repeatability and accuracy. Genrich and Bock [1992] employed a method to filter out the daily repeating multipath signals to show sub-millimeter daily repeatability for ~100 m baselines.

In the following, we study the effects of scattering associated with the receiving antenna, on estimates of geodetic site positioning with GPS. We develop a theoretical model for carrier-phase multipath effects, which follows closely the method and formalism of Young et al. [1985] and of Georgiadou and Kleusberg [1988]. In particular, we assume that the effect of multipath error on the carrier phase signal is described by the reflectivity of the reflecting material and the geometry resultant from the relative position of the transmitting satellite, the reflecting object, and the receiving antenna. We present experimental evidence of the presence of signal-reflection and scattering errors in data acquired from a pillar-mounted GPS antenna (a JPL-type FLINN monument), identical to sites used in the continuously operating International GPS Geodynamics Service (IGS) network. We describe how elevation angle cutoff tests [e.g., Davis et al., 1985] can be used to assess quantitatively the effect of multipath errors on site-position estimates. Finally, we demonstrate that microwave absorbing material reduces the low-frequency component of the multipath error.

Multipath Errors

In making GPS observations, we use low directive gain antennas (of omnidirectional hemispheric coverage design) to acquire data simultaneously from all the visible

satellites, i.e., from satellites in directions of positive elevation angles at the receiving antennas. This design requirement means that reflected signals arriving from any positive elevation angle cannot be rejected. We would nevertheless like to be able to reject entirely all signals arriving from negative elevation angles, as well as all signals with left-hand circular polarization (LCP). As an example, Figure 1 shows a cut through the main lobe axis of the RCP and LCP antenna gain pattern for the L1 frequency of a Dorne-Margolin GPS antenna with concentric choke rings. (Brand names are mentioned for identification purposes only.) This type of antenna/backplane configuration is in common use at sites in the global GPS network. The corresponding L2 antenna-gain patterns are qualitatively similar. The concentric choke rings of these antennas [Tranquilla et al., 1994] have been engineered as a compromise between gain and phase pattern, polarization isolation and portability. The value of the antenna gain below the horizon furthermore represents a balance between the rejection of reflected signals and the acceptance of unreflected signals at low positive elevation angles. From Figure 1 we can see that the gain at an elevation angle of $-45°$, for example, is about 30 dB down relative to the maximum gain at zenith. Thus reflected signals impinging from negative elevation angles are attenuated but not eliminated. To achieve this attenuation, the antenna gain has been gradually reduced toward low positive elevation angles. Since the polarization of the GPS satellite signals will change sign upon each specular reflection, single-reflection (or any odd number reflection) effects can be reduced by antenna polarization discrimination. However, no polarization discrimination is possible for reflected signals reaching the GPS antenna phase center after an even number of reflections. See Schupler et al. [1994] for a characterization of the electrical properties of several different models of GPS antennas used for geodetic measurements.

To quantify the effect of multipath errors on estimated parameters, we must consider the method used to obtain the estimates. Generally, some form of a linear least-squares technique is involved in the GPS data analysis. The basic observables are generally

the ionosphere-free linear combination (LC) of the L1 and L2 phase observables. The pseudo-range observables are sometimes used as well, but they carry little weight relative to the phase observables. In most analyses, the observable used is the so-called "double differenced" LC phase [King et al., 1985], in which between-satellite and between-site differences of the LC phases at each epoch are formed. The clock errors in (1) cancel upon formation of the double differences, and thus clock parameters need not appear in the solution. A different way of dealing with the clock errors is for clock parameters to appear explicitly in the analysis. With this latter technique, a stochastic filter is used to estimate the time-variation of the clock parameters. A stochastic filter can also be used to estimate the atmospheric zenith delays [e.g., Tralli and Lichten, 1990]

The modeling of the atmospheric propagation delay in the analysis of space geodetic data has received a great deal of attention in the last decade, mainly because of its importance in the analysis of VLBI data. Serious attempts to improve the models developed in the late 1960's and early 1970's were made by Davis et al. [1985] and by Lanyi [1984]. More recent models [Herring, 1992; Niell, 1994] are believed to be superior. The main effort was directed towards increasing the accuracy of the so-called mapping function of the hydrostatic delay for low elevation angles ($\lesssim$10°). Systematic errors in the mapping function at low elevation angles were found to be causing errors in the estimates of the vertical coordinate of site position [Davis et al., 1985]. Data from low elevation angles are useful in VLBI, as well as in GPS, to reduce the correlation between estimates of the vertical component of site position and estimates of the corresponding zenith propagation delay.

The problem of the atmospheric propagation delay in the analysis of GPS data is different. Although the technique could in principle benefit from low-elevation angle observations, GPS data are almost always acquired above elevation angles of $\sim$15°-20°, due mainly to the reduced signal-to-noise ratio (SNR) which the antenna pattern imposes on observations from lower elevation angles (see Figure 1) to lessen the

effects of multipath. At such relatively high elevation angles, errors in the atmospheric propagation delay due to the elevation-angle mapping function are usually quite small, always less than 5 mm, and less than 1 mm for nearly all cases [Davis et al., 1985; Lanyi, 1984; Herring, 1992; Niell, 1994]. Horizontal gradients in the wet refractivity of air, as measured by microwave water vapor radiometers, however, may cause azimuth asymmetries of 30 mm in propagation (or "path") delay at an elevation angle of 20° [Davis et al., 1993], but in general systematic errors in models of the atmospheric propagation delay have not been shown to be a major source of error in GPS, if stochastic corrections to the zenith propagation delay are estimated. Nevertheless, when atmospheric propagation delay parameters are estimated, other elevation-angle-dependent systematic errors, non-atmospheric in origin, can be "magnified" because of the high correlations mentioned above.

It has long been understood that multipath errors are greater for data acquired from satellites at lower elevation angle [e.g., Bletzacker, 1985]. Assessments of the effects of multipath on estimates of site position [e.g., Davis et al., 1989] have, however, not generally detected serious effects. The difficulty in developing a quantitative understanding of the effects of multipath has been the inherent dependence of multipath on the radio-reflective environment. Below, we study this situation using a simple model.

Effects of multipath on GPS phase observables

In this section, we develop a model for carrier-phase multipath errors. This development is similar to that presented by Young et al. [1985] and Georgiadou and Kleusberg [1988]. We redevelop the model here to enable examination of its details. Implicit in this model is the fact that the reflecting structure is located in the far field of the antenna so that geometrical (ray) optics, as opposed to physical optics, can be applied.

The model assumes that (1) the incoming GPS signal is a plane wave, and (2) there exists a single planar horizontal reflector, infinitely large, located a distance H beneath the GPS antenna phase center. (We ignore variations of phase center with signal direction; see Schupler et al. [1994].) Under these assumptions, the signal at the antenna phase center is the sum of two signals, the signal arriving from the direct line-of-sight to the satellite, and the reflected signal. Figure 2 illustrates the single-reflector multipath geometry. The signal transmitted by the GPS satellite arriving at the receiving antenna forms an incident elevation angle ϵ with respect to the horizon. The orbital motion of the GPS satellite in the sky relative to the position of the antenna on the ground results in an incident elevation angle $\epsilon(t)$ which is time-dependent. Thus we write the signal, $A(t)$, received at the antenna phase center as the sum of the unreflected signal, $U(t)$, and the reflected signal, $R(t)$:

$$A(t) = U(t) + R(t) \quad . \tag{2}$$

where A, U, and R represent the complex electric or magnetic field of the respective signals. The reflected signal and unreflected signal have the same source, but to reach the phase center, the reflected signal must travel an additional distance $S_1 + S_2$ (see Figure 2), and is attenuated, through reflection and the antenna power pattern, by an amount α, $(0 \leq \alpha \leq 1)$, (assumed real):

$$R(t) = \alpha U(t - \frac{S_1 + S_2}{c}) \tag{3}$$

where c is the speed of light. (We ignore the extra atmospheric propagation delay of the reflected path, which is equivalent to $\lesssim 3$ μm path, and phase and polarization changes which might occur on reflection. Also, for elevation angles $\epsilon < 45°$, the geometry of Figure 2 changes, but the result given below is unchanged.) If we focus on the carrier signal of frequency f, then the unreflected wave may be represented by

$$U(t) = U_o e^{-2\pi i f t} \tag{4}$$

where $U_\circ$ is complex. (The negative sign of the phase is arbitrary and is determined by the way in which the carrier beat phase is defined. Leick [1990], e.g., defines the phase negative to that of equation (1). For a definition of the form of equation (1), the negative sign is appropriate.) Combining (2)–(4), we obtain

$$A(t) = U_\circ e^{-2\pi i f t}\left(1 + \alpha e^{2\pi i \frac{S_1+S_2}{\lambda}}\right) \tag{5}$$

where $\lambda = c/f$ is the wavelength.

From Figure 2, we find

$$\begin{aligned} S_1 &= -S_2 \cos 2\epsilon \\ S_2 &= H \csc \epsilon \end{aligned} \tag{6}$$

The received signal $A(t)$ can also be written in terms of the unreflected signal $U(t)$ and a change in amplitude β and phase $\delta\phi$ as

$$A(t) = \beta U(t) e^{i\delta\phi} \tag{7}$$

where we suppress the time dependence of $U_\circ, \alpha, S_1, S_2, \beta$, and $\delta\phi$ which all vary on the same time.

Comparing (4), (5), and (7), we can express the phase error $\delta\phi(\epsilon; \alpha, H, \lambda)$ as

$$\delta\phi(\epsilon; \alpha, H, \lambda) = \tan^{-1} \frac{\alpha \sin\left[4\pi \frac{H}{\lambda} \sin\epsilon\right]}{1 + \alpha \cos\left[4\pi \frac{H}{\lambda} \sin\epsilon\right]} \tag{8}$$

The multipath error, under the assumptions made above, thus depends on four parameters: the vertical distance, H, from the reflector horizontal plane to the antenna phase center, the attenuation, α, of the voltage amplitude of the reflected signal, the observing wavelength, λ, and the elevation angle, ϵ, of the incident signal.

Before examining the effects of multipath errors in estimates of site position, we present several useful expressions. It is standard in GPS studies to speak of phase not in

radians, as in (8), but in units of length. The multipath phase error expressed in these latter units, which we denote with a subscript L, is thus

$$\delta\phi_L(\epsilon;\alpha,H,\lambda) = \frac{\lambda}{2\pi}\delta\phi(\epsilon;\alpha,H,\lambda) \tag{9}$$

As discussed above, most GPS analyses make use not of the carrier phase observables themselves, but of the ionosphere-free linear combination (LC). Expressed in units of length, the LC multipath phase error for the L1 and L2 frequencies is

$$\delta\phi_L^{\mathrm{LC}}(\epsilon;\alpha,H) \simeq 2.5456 \times \delta\phi_L(\epsilon;\alpha,H,\lambda_1) - 1.5456 \times \delta\phi_L(\epsilon;\alpha,H,\lambda_2) \tag{10}$$

where λ_1 is the L1 wavelength (0.19029 m) and λ_2 the L2 wavelength (0.24421 m). The two constants in (10) are derived from the values for λ_1 and λ_2 [Spilker, 1978]. Figure 3 shows values for the L1, L2, and LC multipath phase errors for $H = 150$ mm and $\alpha = 0.06$. (The reason for these choices will be explained later.) The LC observable as a function of elevation, exhibits a "beating" of the L1 and L2 multipath errors. Constructive "interference" occurs when the L1 and L2 multipath errors are of different sign; destructive interference occurs when the L1 and L2 multipath errors are of the same sign.

This "interference" is more clearly seen in Figure 4, which shows the LC multipath error from (10) for three different choices of H: 0.15 m, 0.60 m, and 1.00 m. The attenuation α is 0.06 in all three cases. When plotted as a function of elevation angle, the multipath error appears sinusoidal with a maximum amplitude proportional to α (for $\alpha \ll 1$); the elevation "wavelength" is proportional to λ/H since, for larger values of H, this sinusoid goes through more cycles between satellite nadir and zenith. Antennas are generally set up 1 m or greater above the ground for tripod setups and for most pillar-mounted antennas. It is usually also possible to set up the antennas at least several meters from other multipath sources (walls, fences, etc...). One might therefore surmise that there is a greater chance for multipath errors to "cancel out"

when averaged over a range of observed elevation angles for larger values of H. Below, we develop a quantitative assessment of the effects of multipath errors on GPS estimates of site position.

Effects of multipath errors on GPS estimates of vertical coordinate of site

We used a simplified analysis to determine the effects of multipath errors. First, we limited our study to least-squares inversions, which are easier to understand than are stochastic filters. We also concentrated on the errors in the estimated vertical coordinate of site position, which, from our discussion above, we suspect that this estimate might be highly influenced by elevation-angle-dependent errors. Further, we did not consider errors in the estimates of satellite orbit parameters. Our model for the observation errors $\delta\phi_L(\epsilon)$ contained three parameters: (1) an ambiguity constant $\delta C_\circ$, (2) an atmospheric zenith propagation delay $\delta\tau_a^z$, and (3) an adjustment to the vertical coordinate of site position δz:

$$\delta\phi_L(\epsilon) = \delta C_\circ + \delta\tau_a^z \csc\epsilon + \delta z \sin\epsilon \tag{11}$$

Effects of multipath on estimates of horizontal position are considered below. When the LC phase multipath errors from (10) are used in the leftside of (11), then the estimates of the parameters in (11) determined by least-squares inversion represent the errors in those parameters caused by the multipath errors.

For the observations, we chose a realistic distribution of elevation angles and we then carried out the least-squares inversion. Figure 5 shows this distribution in a polar coordinate plot; it corresponds to Julian date 15 January 1994, for the Westford GPS site (latitude N 42°61, longitude W 71°49), and a minimum elevation angle of 15°.

We have found that the errors in the estimated parameters strongly depend on the minimum elevation angle used in the solution, the so-called "elevation angle cutoff". Figure 6 shows the errors in the estimated vertical coordinate of site position as a function of minimum elevation angle for the values of H and the value of α

used for Figure 4. We performed elevation angle cutoff tests with and without a zenith delay parameter being estimated. These "cutoff angle" tests demonstrate that (1) the error in this estimate of the vertical coordinate of site position can become dramatically large for reflective objects placed close to the antenna phase-center and for high cutoff angles, and (2) this error becomes "magnified" when a correction to the zenith atmospheric propagation delay is estimated simultaneously. The implications for accurate determination of vertical position, are clear: a small change in the elevation coverage can change the estimates of the vertical coordinate of site position by tens to hundreds of millimeters. Since typical uncertainties for determinations of the vertical coordinate of site position are believed to be $\sim$5 mm, these results indicate that multipath may be a significant source of error.

We have considered how the error in the estimate of the vertical varies when the cutoff angle only is changed. Under the assumptions of our multipath error model and our simplified analysis, if the cutoff angle were to remain fixed over time, then the error in the vertical position estimate would also remain fixed over time, and the error would not affect determinations of site velocity, which are important in a wide variety of crustal deformation studies. Unfortunately, it is not possible to exercise such a degree of control over GPS data acquisition. For example, with the recent onset of Anti-Spoofing (AS) for all the Block II spacecraft, the observations of the precise code signals are no longer possible and some receivers have switched to a cross-correlation mode which in effect decreases the SNR of the phase measurements. To counter this problem, analysts have begun rejecting data obtained from below 20° elevation angle, whereas before AS was implemented data obtained only from below 15° were downweighted. Of course, not only the minimum elevation angle, but any change in the elevation coverage used in the solutions will cause changes in the errors of the parameter estimates. Such a change would occur, for example, if a satellite were to become disfunctional or, if estimates were obtained from observations made during different blocks of sidereal time (the GPS

constellation provides a non-uniform elevation-angle distribution of the visible satellites in the observer's sky).

Systematic errors in estimates of baseline components

In this section, we present experimental evidence of the presence of errors due to signal reflections on estimates of baseline components in data acquired at one site of the permanently operating GPS network. This site (antenna-receiver system and antenna monumentation) is identical to other sites in the continuously operating GPS Global Tracking Network for the IGS (Steven DiNardo, private communication).

In early 1993, the DOSE program of NASA (Dynamics of the Solid Earth) and the National Oceanic and Atmospheric Administration (NOAA) started operating a temporary GPS receiver at Westford (monument WES2), Massachusetts, for the IGS and Fiducial Laboratories for an International Natural Science Network (FLINN). In January 1994, a permanent GPS site was selected at Westford, and its monument erected (monument WFRD). The WFRD antenna is centered over a permanent monument by means of a supporting ring, a spike, and three leveling feet. The monument is a $\sim$1 m high concrete column, 0.75 m in diameter, with a metallic plate 0.45 m in diameter centered on and laid in flush with the top of the concrete. The vertical distance from top of the concrete to the antenna phase center is 0.20 m (Figure 7).

To investigate the radio-reflective environment of the pillar-mounted antenna, a tripod-mounted antenna was set up over another mark, WFR2, a horizontal distance of only $\sim$2.2 m from the WFRD mark. The WFRD and WFR2 GPS systems both consisted of TurboRogue SNR-8000 receivers and Dorne-Margolin antenna-plus-choke ring assemblies. Both the WFRD and WFR2 GPS receivers used the same 5 MHz reference from an external Cesium clock. We used a standard strategy to process the GPS data, samples of undifferenced dual-frequency carrier-phase and pseudo-range measurements obtained every 30 seconds, with the GPS Inferred Positioning System

(GIPSY) software [Webb and Zumberge, 1993, and references therein]. Using the data from each day (starting at 0 UTC), we formed the carrier phase and pseudo-range ionosphere-free linear combination and estimated the three components of position of WFRD relative to WFR2, carrier phase ambiguities, and satellite and station clocks. No tropospheric zenith delays were estimated. Precise orbits and consistent earth rotation parameters were procured from IGS and were not further estimated in the analysis. For a baseline of this length, the ionospheric effects are negligible and use of the ionosphere-free linear combination increases the noise about three- and two-fold relative to the L1 and L2 observables, respectively. Our choice of the "noisier" LC was motivated by the general use of this observable for analyzing data for longer baselines.

The root-mean-square (RMS) postfit LC phase residual was typically ~3 mm, and no systematic patterns were apparent in the phase residuals plotted as a function of time (Figure 8a). When plotted as a function of elevation angle, however, the postfit LC phase residuals displayed a clear systematic dependence (Figure 8b). No azimuth dependence was apparent (Figure 8c). The fact that no signature could be seen when the residuals from all the satellites to a site were plotted versus time or versus azimuth angle indicated that the error was mainly elevation-angle dependent; since the 6–8 satellites visible simultaneously represented a range of elevation angles, the behavior was not visible in a time or azimuth plot involving all the satellites. The systematic behavior was visible in the residuals for any given individual satellite when displayed as a function of elevation angle, or time, or azimuth (Figure 9).

To investigate the possibility that the residuals were caused by a software error, we processed some of the data sets with the Bernese software [Rothacher et al. 1993, and references therein]. This software explicitly uses double-difference data, and hence no clocks are explicitly estimated in the solutions. Otherwise, there should be no difference between the estimates obtained from the two analysis packages. (GIPSY uses a stochastic filter to estimate the time-dependence of the zenith atmospheric

propagation delay, whereas the Bernese software estimates constant values for a given time interval; since we were not estimating these parameters, this difference should not affect the comparison.) The results obtained with the GIPSY and the Bernese software for the baselines investigated were fully consistent. [GIVE SOME QUANTITATIVE EXAMPLES OF AGREEMENTS, DISAGREEMENTS.]

The systematic trend in the residuals repeated itself in data sets from each of several days that spanned more than the following week. Figure 10 shows an example of the postfit LC phase residuals that involve GPS satellite 22 (i.e., PRN 22), observed on April 9 and 10, 1994. The qualitative similarity between the two curves is confirmed quantitatively in Figure 11. The (day-to-day) cross-correlation coefficient function for the time series shown in Figure 10 peaks at a value of 0.705 at a delay time of 4 min. For an error that depends solely on satellite position, the cross-correlation peak should occur ~3.93 min later on each successive day, since the satellite constellation repeats itself once per sidereal day. The data of Figure 10 were recorded, as described above, every 30 seconds, which is therefore the resolution of the curve in Figure 11. The repeating signature can be removed by differencing the residuals, adjusting for the daily ~4-min advance. The RMS scatter of the differenced residuals is 1.8 mm, whereas if the two data sets were independent, the RMS scatter of the difference should be the root-sum-square of the RMS residual from each of the two days, or 2.7 mm. The high degree of day-to-day correlation demonstrates that the error causing the systematic behavior is associated with repeated satellite-to-antenna geometry. The two sources of error that meet this criterion are signal reflections/multipath and antenna phase-center variations.

Antenna phase-center variations are due to the non-sphericity of the antenna phase pattern and, therefore, are independent of the antenna environment. Schupler et al. [1994] used an anechoic chamber to measure the L1 and L2 phase pattern, phase center location, amplitude pattern, and axial ratio pattern of several different models

of GPS antennas used for geodetic measurements, and demonstrated that each of the antennas displays anisotropic phase-center variations at the centimeter level (a few degrees of phase at L-band). For the type of antenna used in the experiments presented in this paper, the Dorne-Margolin antenna with choke ring, the phase pattern is nearly isotropic, with RMS azimuthal variations at the 1–2 mm level; by contrast, phase center variations amount to ~10–14 mm, peak-to-peak, over an elevation range of 0–90°. If the phase pattern is similar for all antennas of the same make and model (microstrip patch antennas, like Dorne-Margolin, are manufactured with very repeatable techniques and Schupler et al. [1994] concluded that variations between such antennas are insignificant for geodetic purposes), then for this short-baseline experiment we would not be sensitive to phase-center variations because the difference in elevation angles from the ends of a ~2.2 m baseline for a given satellite at a given epoch is negligible. To investigate the possibility that the antenna phase patterns are different, we switched the GPS antennas (but not the receivers) of the WFRD and WFR2 sites. The WFR2 antenna was mounted on a standard surveying tripod, and both receivers were connected to the same external 5 MHz reference. With the antennas switched, we again processed the data from this baseline. If the source of the error were antenna-dependent, then the error should change signs when the antennas are switched. The results, however, were unchanged. We also tried switching receivers, and the results were again unchanged. The results of these tests led us to believe that the effect was caused by the environment specific to the WFRD antenna. We tentatively concluded that the effect was caused by scattering and reflections from the WFRD pillar-antenna combination, since data obtained from the WFR2 site, only 2.2 m away, did not seem to suffer from these effects. Additional support to this conclusion also came from analysis of the WES2-WFRD and WES2-WFR2 baselines. (WES2 is located ~580 m to the north-east of both WFRD and WFR2 and consists of the same antenna-receiver system.) We processed the data from these two baselines independently; the elevation-angle-dependent error was associated

a) Mention that WES2 has also problems?

to WFRD. b) Include MILL, INTL (= baseline triads) to support argument

In order to further quantify the elevation-angle-dependent error, we performed cutoff angle tests. Using our study described above, we should be able to relate the results of the cutoff angle test to parameters in the multipath model (H and α) under our hypothesis of reflections from the surface of the pillar. Figure 12 contains the results from the cutoff angle tests. Plotted are the values, relative to those for the 5° cutoff angle solution, of the estimates of the north, east, and vertical components of the ~2.2-m WFRD–WFR2 baseline, as a function of minimum elevation angle. The error bars are the statistical standard deviations of the differences [Davis et al., 1985], based on our adopted standard deviations of 3 mm for the LC phases, typical values for the RMS postfit LC phase residuals (see above). For this short-baseline test, no zenith atmospheric propagation delay parameters were estimated. The cutoff angle test results of Figure 12 display significant, centimeter-level, systematic deviations from zero for the estimates of the vertical component; the results for the horizontal components show insignificant deviations from zero.

The results of the cutoff angle tests show qualitative similarities to those determined from the simulations for values of H and α in the ranges 100–200 mm and 0.05-0.10, respectively. The simulations, however, fail to reproduce the results of the cutoff angle tests for minimum elevation angles $\lesssim 20°$; the inflection in the estimate of the vertical component at about 20° seen in Figure 6a is not present in Figure 12.

As a further test of our multipath model, we used our simulation approach to calculate values of postfit LC phase residuals. Although this check is not completely independent, since the data used to generate the cutoff angle test and the postfit LC phase residuals are the same, neither is it completely redundant, for no one-to-one relation exists between the postfit residuals and the results of the cutoff angle test. In Figure 13, we present the postfit residuals from this simulation for $H = 130$ mm and $\alpha = 0.1$ along with the observed postfit LC phase residuals. We also present this

comparison in Figure 13 for a single satellite. The model reproduces the long time-scale (several hours) behavior quite well, but fails to account for the higher frequency variations.

In deriving the multipath model of the previous section, we assumed that ray (geometric) optics could be used. Such an assumption is valid when the reflecting structure is located in the far-field of the antenna. The boundary between the near-field or Fresnel zone and the far-field or Fraunhoffer zone of an antenna can be determined using the expression [Kraus, 1988],

$$R = 2L^2/\lambda \tag{12}$$

where R is the distance from the antenna phase center to the boundary, L is the maximum dimension of the antenna, and λ is the observing wavelength. For the Dorne-Margolin antenna with choke ring groundplane (L = 381 mm; LC equivalent-λ = 107 mm) R = 2.7 m. Because the vertical distance from the top surface of the WFRD pillar to the antenna phase center is only ~0.2 m, the reflecting structure is located in the near-field of the antenna, difraction and scattering effects from its edges may be of significant contribution, and therefore, the problem should be regarded as one of physical optics. The multipath model, based on geometrical optics, provides, however, a convenient approximation.

Based on the qualitative and quantitative similarities between the results from the cutoff tests for the WFRD-WFR2 data and from the simulation, and on the similarities between the postfit residuals obtained from the WFRD-WFR2 analyses and from the simulation, we hypothesized that the source of the elevation-angle-dependent error is scattering from the antenna and pillar surfaces and reflection from the top of the pillar. In the next section we describe an experiment that tested this hypothesis.

The Use of Microwave Absorbing Material for Reducing Multipath Effects

The preceding section indicates that modeling accurately the multipath error of an actual antenna environment can be extremely difficult. Instead of modeling, we therefore tried to establish the main cause of the multipath error via a controlled experiment. We processed LC measurements from the WFRD-WFR2 baseline with WFRD having acquired data in two different configurations: with and without microwave absorber material placed on top of the WFRD pillar. The microwave absorber material covered the pillar and the steel plate embedded in it, and was below the choke rings attached to the Dorne-Margolin antenna of the WFRD TurboRogue (Figure 14). Figure 15 shows the postfit LC phase residuals versus elevation angle of WFRD from the ~2.2-m baseline as obtained over two consecutive days: top, the monument not covered with microwave absorber material; bottom, the monument covered with microwave absorber material. The postfit LC phase residuals display a systematic dependence on elevation angle in the top plot; this dependence is not evident in the bottom plot. Figure 16 shows the difference in the RMS of the postfit LC phase residuals of the top and bottom plots of Figure 15 with binning of the data in 1° elevation-angle increments. The RMS residuals are reduced, in a root-sum-square sense, by about 2 mm at elevations $\gtrsim 75°$, and about 1 mm elsewhere. Figure 17 shows the results from the cutoff angle tests performed on these two data sets; as expected based on the residuals, the systematic deviations from zero of the estimates of the vertical component, present when the monument is not covered with absorber material, are significantly reduced when absorber material is employed.

Four other geometrical shapes and configurations of microwave absorber material were tested, namely, two layers of absorber instead of one, the absorber extended well over the diameter of the pillar instead of tailored to it, absorber covering only the steel plate embedded in the pillar and not the concrete pillar itself, and vice versa. These all proved to be comparably effective at reducing the long period (low frequency) multipath,

but the first two configurations are somewhat more effective than the last two.

Effects on Estimates of Horizontal Coordinates

The results of the elevation angle cutoff test of Figure 12 indicated that the estimates of the horizontal coordinates of site position are not significantly affected by the scattering and reflection of the GPS signals. In order to test this result, we performed simulations as before except that our observational model (11) was modified to include parameters for the horizontal coordinates. For the distribution of observations used in the previous simulations, the new simulations indicated that the predicted errors in the estimates of the horizontal coordinates were less than 0.4 mm for the north component and less than 0.2 mm for the east component. This results can be understood qualitatively by examining Figure 5, which indicates that over the 24-hr observing period, the satellites rise and set over a wide range of azimuths. Thus, if the line of sight over a particular range of azimuths were blocked, then the errors in the horizontal coordinates may not be as small. We have not tested this hypothesis, however.

Discussion and Conclusions

We have used a simple (ray tracing) theoretical model to study the effects of carrier-phase multipath errors on estimates of site positions. This multipath model depends on four quantities: the vertical distance from a horizontal reflecting surface to the antenna phase center, the average amplitude attenuation factor for the reflected signal, the observing wavelength, and the elevation angle of the incident signal. Antenna-phase-center variations are a second order effect and are not included in this model. This model shows that the estimate of the vertical coordinate depends strongly on the minimum elevation angle of the data used in the analysis. The error in this estimate can become dramatically large for reflective objects placed close to the antenna

phase-center, due to its low frequency nature at small ($\lesssim$0.2 m) heights, and for high elevation angles. The error in the estimate of the vertical coordinate is further amplified when atmospheric propagation delays at zenith are estimated simultaneously with site position.

We found that the postfit LC phase residuals for a pillar-mounted permanent GPS antenna at Westford, Massachusetts, displayed a systematic dependence on elevation angle. The maximum of the day-to-day cross correlation of these residuals, at a time delay of approximately 4 min, demonstrated that the error causing the systematic trend was associated with the satellite-antenna geometry. The results from the elevation angle cutoff tests performed on these data displayed significant, centimer-level changes in the estimates of the vertical component, but insignificant changes for the horizontal components, of site position. Simulations based on values for the parameters of the multipath model, $H = 130$ mm and $\alpha = 0.1$, reproduce well the long time-scale behaviour of the observed postfit LC phase residuals. To test the hypothesis that the source of the elevation-angle-dependent effect was reflections from the top of the pillar, we placed microwave absorber material between the antenna choke ring and the monument. The postfit LC phase residuals and the results from elevation angle cutoff tests for a data collected from both ends of a $\sim$2.2-m-long baseline with the microwave absorber in place, verified the hypothesis and demonstrated the ability to reduce, by about 75%, the error in the estimate of the vertical coordinate of site position, caused by multipath effects. Extensions of the chocke ring groundplane structure by adding some more corrugations of varying radius and perhaps rolled-antenna edges may be more effective in reducing multipath and edge scattering effects than the use of microwave absorbing material. This other possibility is currently being investigated at Chalmers University and will be reported elsewhere. The Wesford WFRD GPS site with this FLINN monument is identical to other sites of the continuously operating IGS network.

The implication of these results for vertical GPS positioning are clear: the

GPS constellation provides a non-uniform distribution of the visible satellites in the observer's sky, and a small change in the elevation coverage can change the results significantly, primarily the estimate of the vertical component of site position. For example, some analysis centers of the GPS community currently processes data with a minimum elevation angle of about 20° when AS is in effect, instead of 15° when it is not. The change in the estimate of the vertical component of site position at Westford WFRD introduced by such a small change in the processing strategy is 2.7±0.4 mm (cf. Figure 12). The lifetime and availability of the GPS satellites is not subject to the users' control, and therefore the satellite elevation-angle distribution can change involuntarily; there are also conditions that can be changed voluntarily such as antenna monumentation, backplane structures used, etc. The changes in the estimates of the vertical of GPS antennas can be as much as hundreds of millimeters under some of these circumstances.

Permanent GPS antennas, including those of the global tracking network, are most often emplaced atop durable, stable monuments designed and built by different countries and agencies, yet they show common features. Many sites consist of 1-3 m high concrete pillars atop which GPS antennas mount directly onto bolts set into the monuments. Unfortunately, data acquired at many of the sites of the global GPS network mounted this way, have been seen to present similar elevation-angle-dependent effects. Multipath effects on the carrier-phase signal caused by the monument supporting the GPS antenna is most likely the source of this error; the period and amplitude of the multipath signal, though sometimes similar at a variety of sites, is dependent upon the particular multipath environment. Estimates of the vertical component of site positions from GPS networks over all scales can be affected at the centimeter level by multipath signals. This systematic error may be present in the data from most of permanent GPS sites around the world. For example, data acquired from a permanent GPS network established in Sweden for measuring the three dimensional deformation associated with

glacial isostatic adjustment [e.g., Mitrovica et al., 1994; Johansson et al., 1994] supports this suspicion. The pathologies found in some of these data resemble those found at the Westford site, which were shown to be caused primarily by reflections from the permanent monument. This network – SWEPOS – (Swedish permanent GPS array) consists of twenty sites, fifteen of which are equipped with TurboRogue GPS receivers and Dorne-Margolin antennas with chocke ring groundplane, established all along and across Sweden. This regional network comprises baselines that range in length between 100 and 1500 km and has been continuously operating since August 1993.

Estimates of the vertical component of Onsala shown a discontinuous change on January 31, 1994 when AS was activated and, consequently, the minimum elevation angle of acceptable data was changed from 15° to 20°. (Onsala is a site of both this network and the GPS Global Tracking Network for the IGS.) The postfit LC phase residuals from this site display a systematic effect dependent on elevation angle. Results from elevation angle cutoff tests display systematic deviations from zero for the estimates of the vertical component of this site. None of these pathologies can be seen in the data from the other sites. Why? To insure stability of the monuments over time scales of several years, all the permanent GPS antennas in the SWEPOS network, except Onsala's, are emplaced atop a platform on a 3-m tall concrete pillar. Onsala's monument, on the other hand, is only about 1-m tall, and is hexagonal instead of cylindrical. The use of microwave absorber material at the Onsala site has served to verify the suspicion of presence of signal multipath associated with this site's monument and to partially reduce the error, the remaining error most likely being caused by multipath problems at the other monument sites. The absence of these pathologies for the other sites is possibly a manifestation of the degree of cancellation of common multipath errors (the maximum difference in elevation angle to the same satellite as seen simultaneously from the two ends of a 400 km-long baseline is only 2°). We hypothesize that if this homogeneous network were of global scale, instead of regional, the error

would also be present.

We have found additional problems with vertical positioning from GPS data acquired at sites of this continuously operating network where heavy snow occurs. The effects have the characteristics observed for multipath and could be interpreted as being related to changes in the multipath pattern due to changes in the amount and the type of snow temporarily accumulated in the surroundings of a GPS antenna. A thorough analysis and quantitative assessment of all kinds of systematic errors, such as multipath effects, antenna-phase center variations, and atmospheric loading, in the daily estimates of site positions from this network will be presented elsewhere.

All the results presented here were obtained with only one type of antenna. The multipath error depends not only on the particular satellite-antenna geometry of a given site, but also on the antenna electrical characteristics; thus, different antennas will present different multipath characteristics.

Acknowledgements: We would like to thank M. Chin of NOAA for allowing us to perform tests with the Westford (WFRD) GPS antenna and for providing an additional GPS system. M. Poirier assisted in the installation and operation of the GPS systems. M.L. Exner of UCAR for providing the data of Figure 1. E. Tong, R. Blundell, and C. Papa for useful discussions and for providing microwave absorber material for initial tests. Ph. Raffin for his assistance with Figure 14. We wish to thank P.-S. Kildal for useful discussions about the electrical properties of microwave antennas. We gratefully acknowledge the facilities of the Submillimeter Array (SMA) of the Smithsonian Institution at Westford which were made available to us. This work was supported by the Smithsonian Institution, NSF grant EAR-9105502, and NASA grant NAG5-538.

References

Bletzacker, F.R., Reduction of multipath contamination in a geodetic GPS receiver, *Proc. First Symp. on Precise Positioning with the GPS*, Rockville, MD, April 15–19, 413–422, 1985.

Blewitt, G., Advances in Global Positioning System technology for Geodynamics investigations: 1978-1992, in Contributions of Space Geodesy to Geodynamics: Technology, edited by D.E. Smith and D.L. Turcotte, pp. 195-213, Geodyn. Ser. vol. 25, AGU, Washington, D.C., 1993.

Counselman III, C.C., and I.I. Shapiro, Miniature interferometer terminals for earth surveying, *Bull. Geod.*, *53*, 139–163, 1979.

Counselman III, C.C., and S.A. Gourevitch, Miniature interferometer terminals for earth surveying: ambiguity and multipath with Global Positioning System, *IEEE Trans. Geosci. Remote Sens.*, *GE-19*, 244–252, 1981.

Davis, J.L., T.A. Herring, I.I. Shapiro, A.E.E. Rogers, and G. Elgered, Geodesy by radio interferometry: Effects of atmospheric modeling errors on estimates of baseline length, *Radio Science*, *20*, 1593–1607, 1985.

Davis, J.L., W.H. Prescott, J.L. Svarc, and K. Wendt, Assessment of Global Positioning System measurements for studies of crustal deformation, *J. Geophys. Res.*, *94*, 13,635–13,650, 1989.

Davis, J.L., G. Elgered, A.E. Niell, and C.E. Kuehn, Ground-based measurement of gradients in the "wet" radio refractivity of air, *Radio Science*, *28*. 1003–1018, 1993.

Dixon, T.H., An Introduction to the Global Positioning System and some geological applications, *Rev. Geophys.*, *29*, 249–276, 1991.

Evans, A.G., and J.T. Carr, Effect of signal multipath errors at DMA Global Positioning System satellite tracking sites on orbit accuracy, *Manuscripta Geodaetica*, *14*,

143–148, 1989.

Genrich, J.F., and Y. Bock, Rapid resolution of crustal motion at short ranges with the Global Positioning System, *J. Geophys. Res.*, *97*, 3261–3269, 1992.

Georgiadou, Y., and A. Kleusberg, On carrier signal multipath effects in relative GPS positioning, *Manuscripta Geodaetica*, *13*, 172–179, 1988.

Greenspan, R.L., A.Y. Ng, J.M. Przyjemski, and J.D. Veale, Accuracy of relative positioning by interferometry with reconstructed carrier GPS: Experimental results, *Proc. 3rd International Symp. Sat. Doppler Positioning*, Las Cruces, NM, February 8-12, 1177–1195, 1982.

Herring, T.A., Modeling atmospheric delays in the analysis of space geodetic data, in *Refraction of Transatmospheric Signals in Geodesy*, edited by J.C. De Munck and T.A.Th. Spoelstra, Netherland Geodetic Commission Publications in Geodesy, *36*, 157–164, 1992.

Johansson, J.M., R.T.K. Jaldehag, T.R. Carlsson, T.M. Carlsson, G. Elgered, P.O.J. Jarlemark, B.I. Nilsson, B.O. Rönnäng, H.-G. Scherneck, J.L. Davis, P. Elósegui, and J.X. Mitrovica, Fennoscandian post-glacial land uplift: results from seven months of continuous GPS observations, *J. Geodyn.* (submitted) 1994.

King, R.W., E.G. Masters, C. Rizos, A. Stolz, and J. Collins, Surveying With Global Positioning System GPS, 128 pp., Dummler, Bonn, 1985.

Kraus, J.D., Antennas, McGraw-Hill Book Company, second edition, 1988.

Lanyi, G., Tropospheric calibration in radio interferometry, in *Proc. of the Int. Symp. on Space Techniques for Geodynamics*, edited by J. Somogyi and Ch. Reigber, p. 184, IAG/COSPAR, Sopron, Hungary, 1984.

Leick, A., GPS satellite surveying, John Wiley & Sons, Inc., 1990.

Liebe, H.J., An updated model for millimeter wave propagation in moist air, *Radio Science*, *20*, 1069–1089, 1985.

Mitrovica, J.X., J.L. Davis, and I.I. Shapiro, A spectral formalism for computing

three-dimensional deformations due to surface loads, 2. Present-day glacial isostatic adjustment, *J. Geophys. Res.*, *99*, 7075–7102, 1994.

Niell, A.E., The best mapping function in the world, (In preparation) 1994.

Rothacher, M., G. Beutler, W. Gurtner, E. Brockmann, and L. Mervart, Bernese GPS software version 3.4, *Univ. of Berne*, Switzerland, 1993.

Schupler, B.R., R.L. Allshouse, and T.A. Clark, Signal characteristics of GPS user antennas, *Navigation*, in press, 1994.

Spilker, J.J., GPS signal structure and performance characteristics, *Nav. J. Inst. Nav.*, *25*, 121–146, 1978.

Tralli, D.M., and S.M. Lichten, Stochastic estimation of tropospheric path delays in Global Positioning System geodetic measurements, *Bull. Geod.*, *64*, 127–159, 1990.

Tranquilla, J.M., Multipath and imaging problems in GPS receiver antennas, *Proc. 4th International Symp. Sat. Positioning*, Austin, TX, 557–571, 1986.

Tranquilla, J.M., S.R. Best, and B.G. Colpitts, Selection and application criteria for GPS receiver antennas, *CGU annual meeting*, Ottawa, On., May 19-21, 1986.

Tranquilla, J.M., J.P. Carr, and H.M. Al-Rizzo, Analysis of a choke ring groundplane for multipath control in Global Positioning System (GPS) applications, *IEEE Trans. Antennas Propagat.*, *42*, 905–911, 1994.

Wells, D., N. Beck, D. Delikaraoglou, A. Kleusberg, E.J. Krakiwsky, G. Lachapelle, R.B. Langley, M. Nakiboglou, K.-P. Schwarz, J.M. Tranquilla, and P. Vaníček, *Guide to GPS Positioning*, Canadian GPS Associates, Fredericton, NB, 1986.

Young, L.E., R.E. Neilan, and F.R. Bletzacker, GPS Satellite Multipath: An Experimental Investigation, *Proc. First Symp. on Precise Positioning with the GPS*, Rockville, MD, 423–432, 1985.

Webb, F.H. and J.F. Zumberge, An Introduction to the GIPSY/OASIS-II, *JPL*

Opps!!

Publication, Jet Propulsion Laboratory, Pasadena, CA, 1993.

This manuscript was prepared with the AGU LaTeX macros v3.0.

Figure 1. Right- and left-hand circular polarization antenna gain pattern, on a decibel scale, for the L1 frequency for a Dorne-Margolin GPS antenna with choke rings. The 3-dimensional gain patterns are a figure-of-revolution of it around the main-lobe axis. Data obtained from ~~B.R. Schupler and/or~~ M.L. Exner (personal communication). I failed to win today. He'll be happy to provide the data. Will send them by tomorrow.

Figure 2. Diagram of single-reflector geometry for multipath model ($\epsilon \geq 45°$).

Figure 3. Multipath phase errors for the L1 (dotted), L2 (dashed) and LC (dot-dashed) phase observables, in units of length as per (9), based on the multipath model (8) and (10). The calculations used $H = 150$ mm and $\alpha = 0.06$

Figure 4. LC multipath error for $\alpha = 0.06$ and for three values of the parameter H: (a) $H = 0.15$ m; (b) $H = 0.6$ m; and (c) $H = 1$ m.

Figure 5. GPS satellite position plot for the Westford site (latitude N 42°61, longitude W 71°49) for 24 hours. The zenith point (ϵ=90°) corresponds to the center of the plot, the horizon (ϵ=0°) to the outer circle.

Figure 6. Estimate of the vertical coordinate of site position as a function of minimum elevation angle, relative to the estimate for a 5° minimum elevation angle ("elevation angle cutoff test") for the multipath phase error model and the elevation-azimuth distribution of Figure 5, without (a) and with (b) simultaneous estimate of zenith atmospheric propagation delay. The calculations used $\alpha = 0.06$ and three values of the parameter H: $H = 0.15$ m (dashed); $H = 0.6$ m (dotted); and $H = 1$ m (solid).

Figure 7. Photographic reproduction of the WFRD permanent GPS antenna and monument, located at Westford, Massachussets. (AEN said he'd have it ready (blueprint) by tomorrow).

Figure 8. Postfit LC phase residuals for the 2.2-m-long WFRD-WFR2 baseline, plotted as a function of (a) time; (b) elevation angle; and (c) azimuth. Data were acquired every 30 sec for 24 hours on April 9, 1994.

Figure 9. Same as Figure 8, except data from satellite pseudo-random-noise (PRN) P-code number PRN 22 are shown.

Figure 10. LC phase residuals for the 2.2-m-long WFRD-WFR2 baseline from PRN 22 for ~5 hr on each of two consecutive days: (a) April 9, 1994 and (b) April 10, 1994.

Figure 11. Cross correlation for the two time series shown in Figure 10. The cross correlation is a maximum for $\tau = 240$ s, with a peak value of $\rho = 0.705$. The dashed lines indicate the range between which the cross correlation should fall 99% of the time, under the hypothesis that the data from the two days are uncorrelated.

Figure 12. Example of elevation angle cutoff test for the WFRD-WFR2 data obtained on April 17, 1994. Results are shown for the three local geodetic components of position of the WFRD antenna: North (solid), East (dashed), and Up (dotted). The position of the WFR2 antenna was held fixed, and no zenith atmospheric propagation delay parameters were estimated. The error bars are the statistical standard deviations of the differences (see text) between the indicated solutions and the 5° solution, for an assumed a 10 mm uncertainty for each LC phase measurement.

Figure 13. (a) LC phase residuals for the WFRD-WFR2 baseline for all satellites from the April 9, 1994 data, plotted as a function of elevation angle. The gray line shows the simulated residuals based on the simple multipath model with values of $H = 130$ mm and $\alpha = 0.01$. (b) Same as (a), except that residuals for satellite PRN 22 only are shown, only every 10th data point is shown, and the residuals are plotted as a function of time. (c) Same as (b), except the residuals are plotted as a function of azimuth.

Figure 14. Photograph of the WFRD permanent GPS antenna and concrete monument (foreground) with the microwave absorber in place, and the WFR2 antenna on the wooden tripod (background).

Figure 15. Comparison of LC phase residuals for the WFRD-WFR2 baseline acquired (a) April 17, 1994, when no microwave absorber was used; and (b) June 11, 1994, when the microwave absorber shown in Figure 14 was in place.

Figure 16. (a) Root-mean-square values of the LC phase residuals for the WFRD-WFR2 baseline binned in elevation angle (bin width of 1°) for the data shown in Figure 15: April 17, 1994, no microwave absorber (grey); June 11, 1994, microwave absorber in place (black). The root difference squared and the average of the number of data points used to estimate values in (a) are plotted in (b) and (c), respectively.

Figure 17. Difference in estimates of the vertical coordinate of site position at WFRD from elevation angle cutoff tests for the data shown in Figure 15: April 17, 1994, no microwave absorber (solid); June 11, 1994, microwave absorber in place (dashed); the ordinate origin is defined by the estimate for a 5° elevation angle cutoff with the microwave absorber in place. The error bars are as explained in Figure 12.

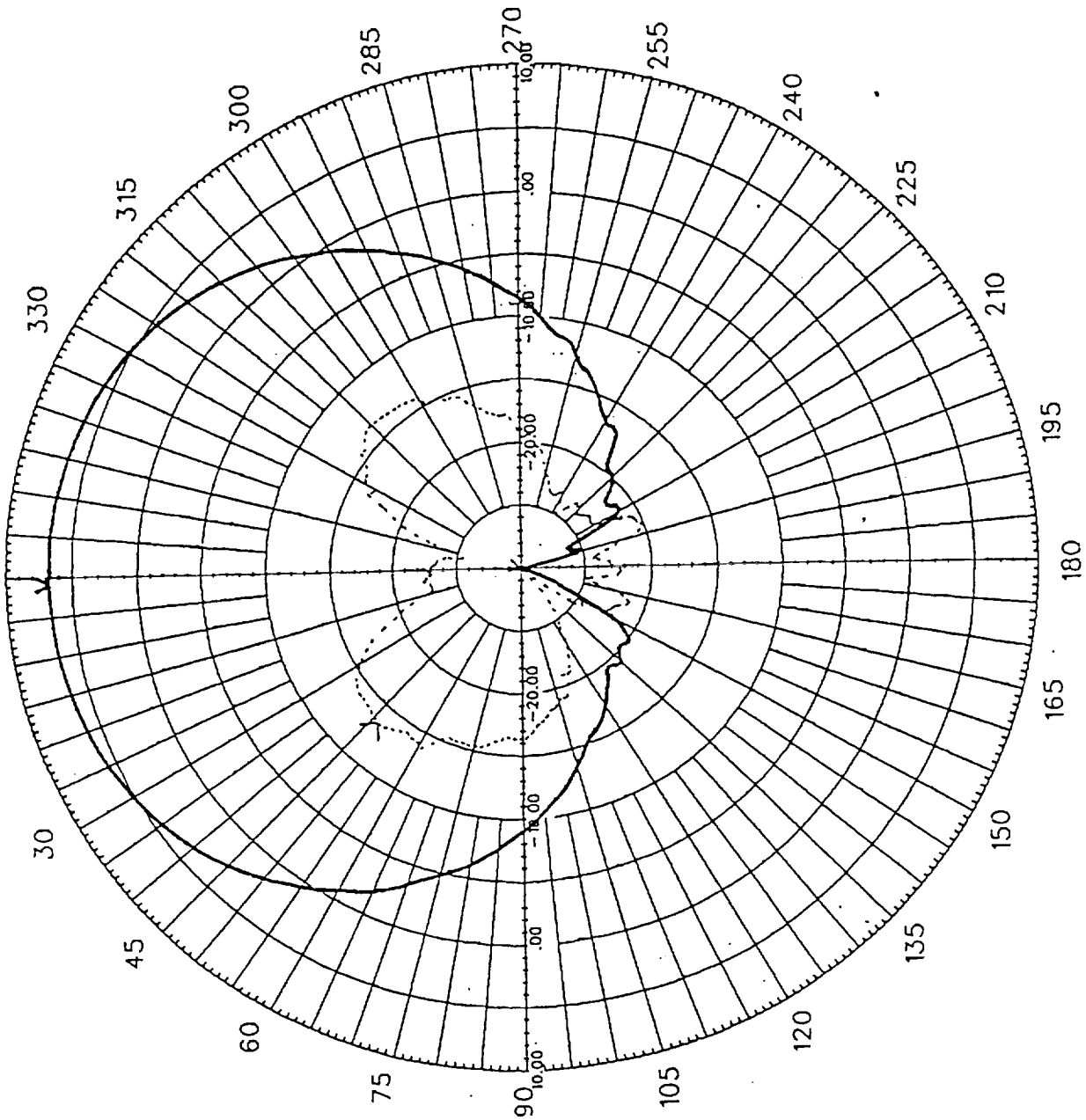
0
15
30
45
60
75
90
105
120
135
150
165
180
195
210
225
240
255
270
285
300
315
330
345
10.00
.00
-10.00
-20.00
-30.00
-10.00
.00
10.00

Fig 1

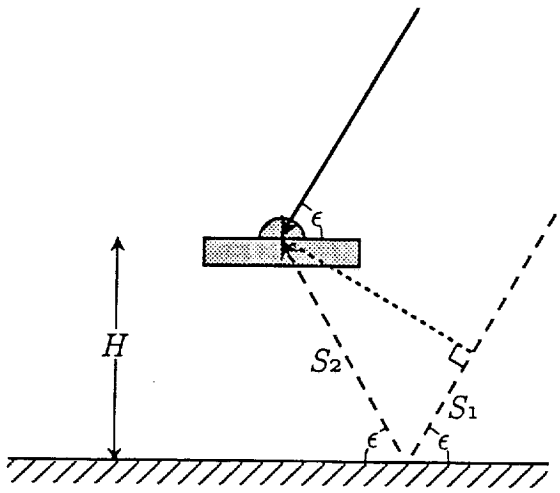

Fig 2

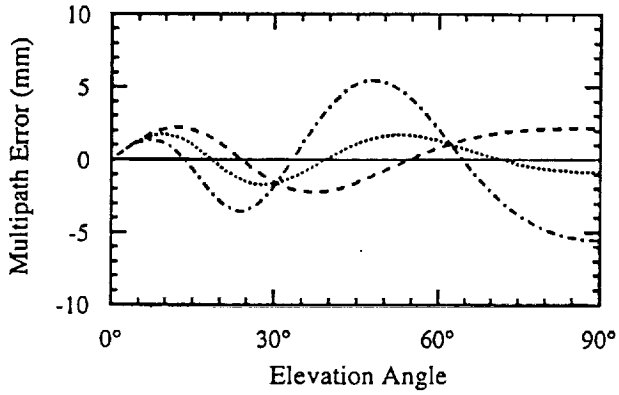

Fig 3

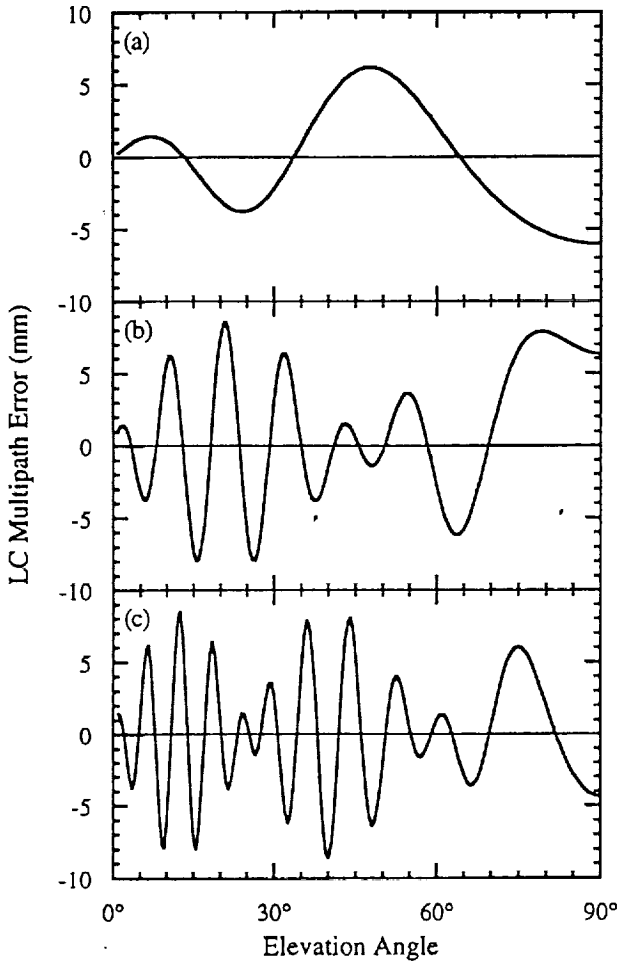

Fig 4

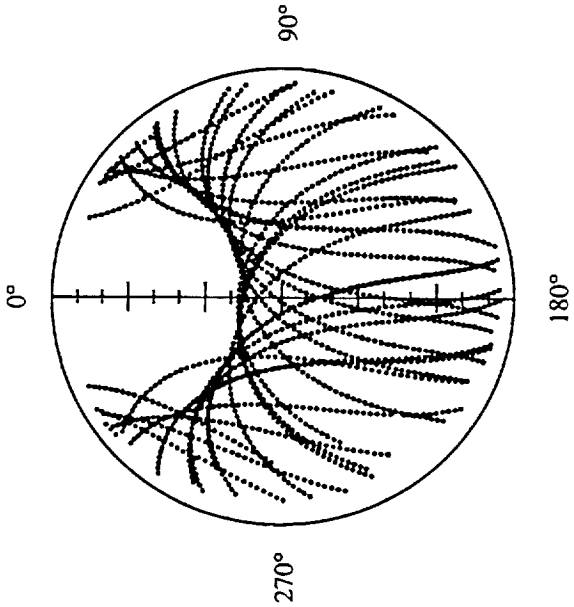

FIG 5

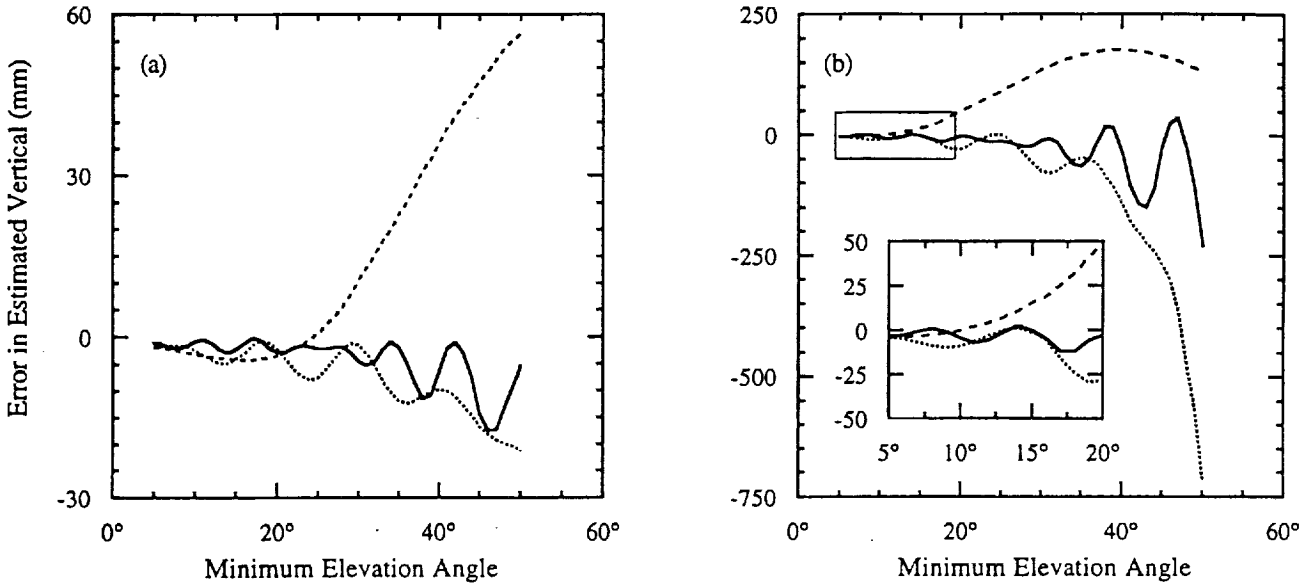
(a)
60
30
0
-30
Error in Estimated Vertical (mm)
0°
20°
40°
60°
Minimum Elevation Angle
(b)
250
0
-250
-500
-750
50
25
0
-25
-50
5°
10°
15°
20°
0°
20°
40°
60°
Minimum Elevation Angle

Fig 6

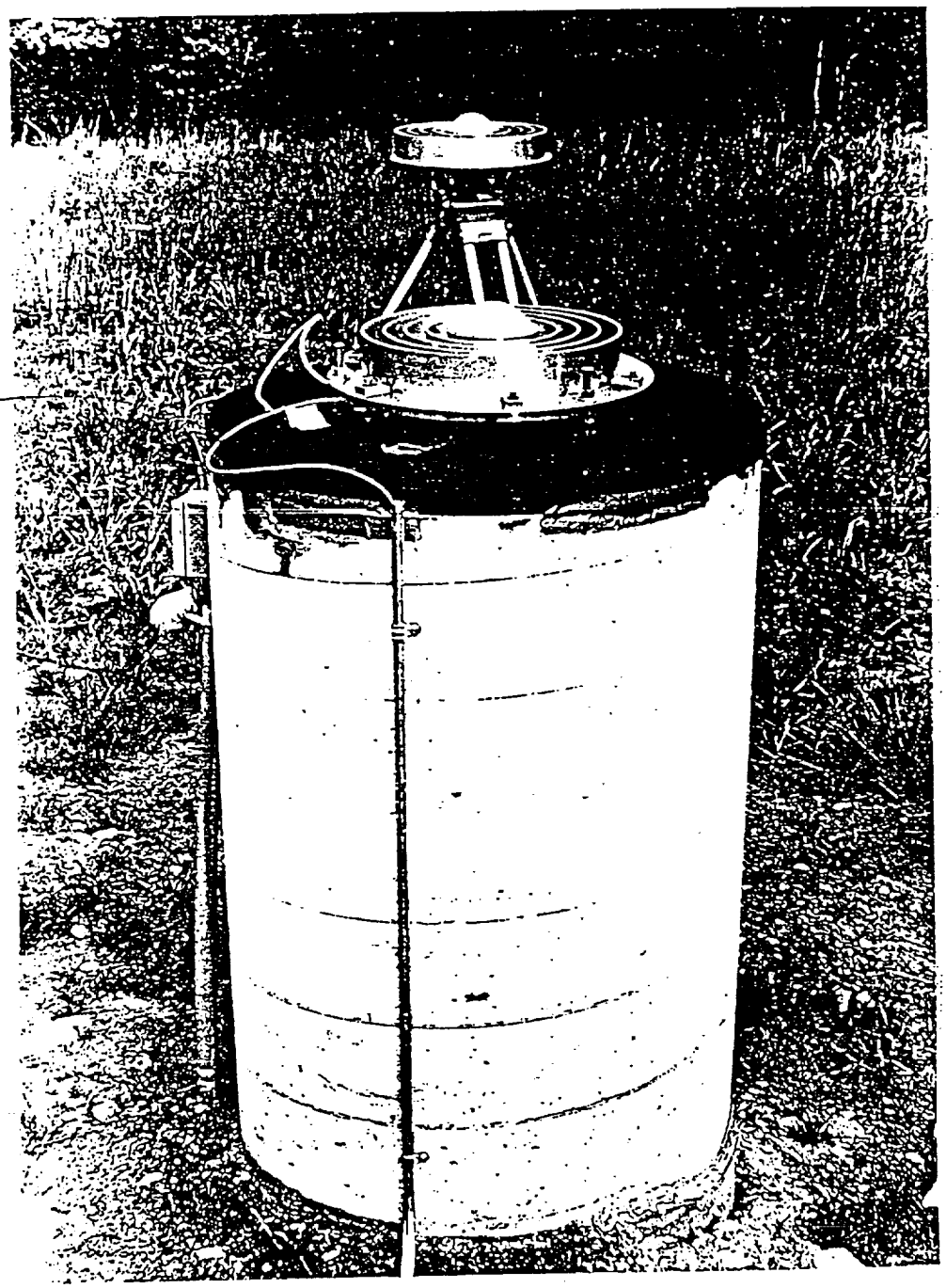

Get a picture of LUFRI without the microwave absorber material covering top of the pillar.
(AEN)

(requested)

Fig 7

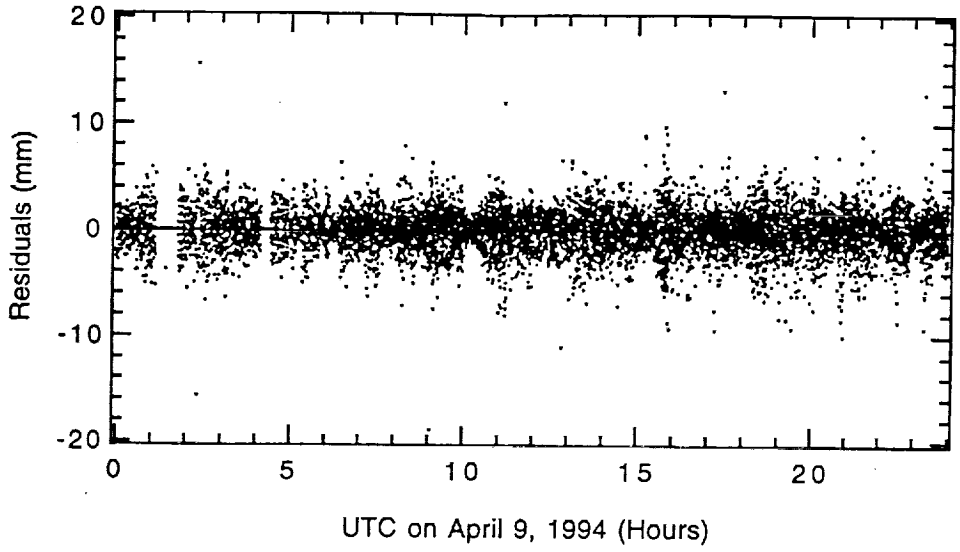
Residuals (mm)
20
10
0
-10
-20
0
5
10
15
20
UTC on April 9, 1994 (Hours)

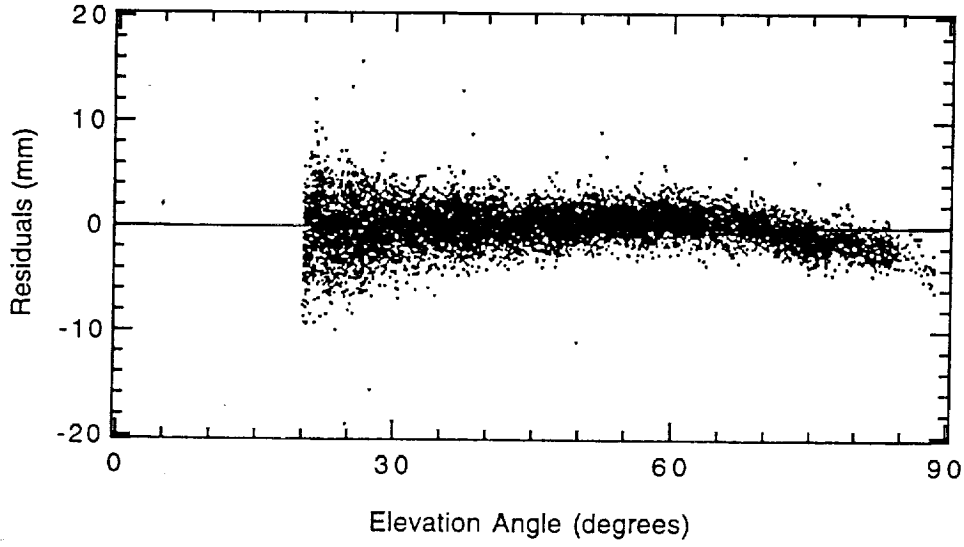
Residuals (mm)
20
10
0
-10
-20
0
30
60
90
Elevation Angle (degrees)

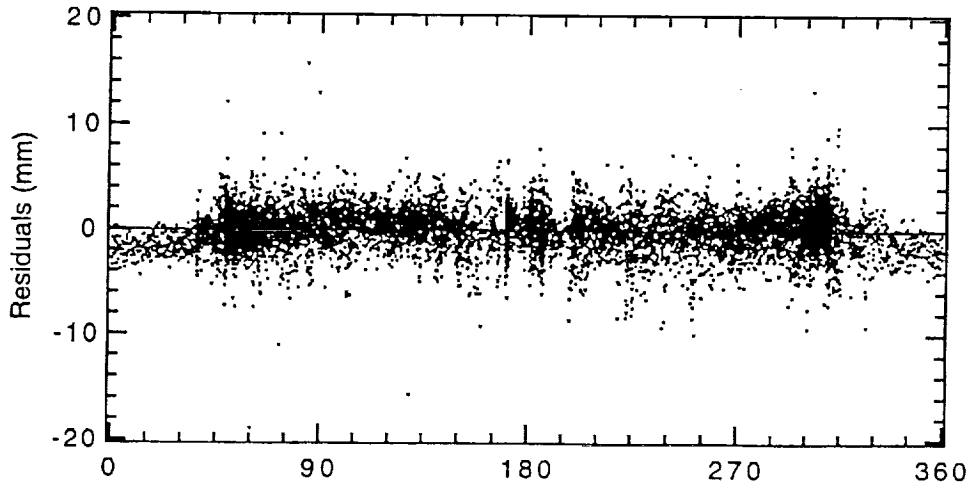
Residuals (mm)
20
10
0
-10
-20
0
90
180
270
360
Azimuth Angle (degrees)

Fig 8

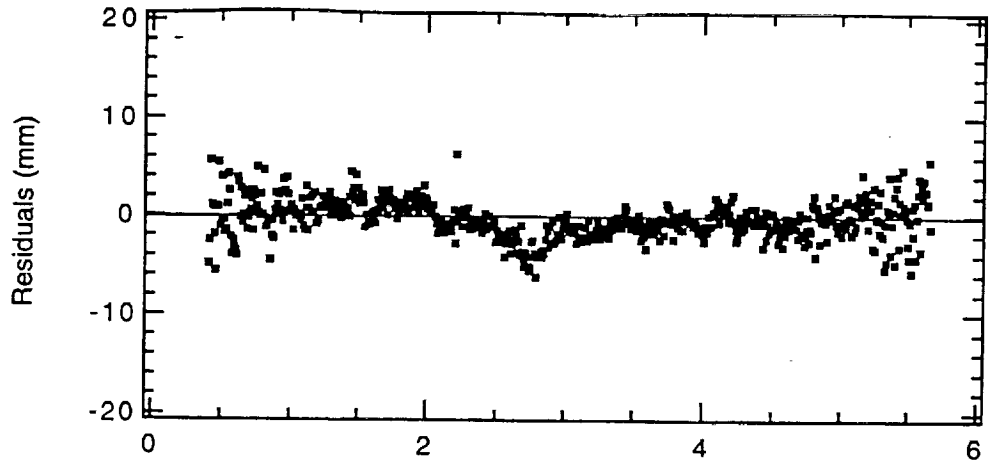
Residuals (mm)
20
10
0
-10
-20
0
2
4
6
UTC on April 9, 1994 (Hours past 13:00)

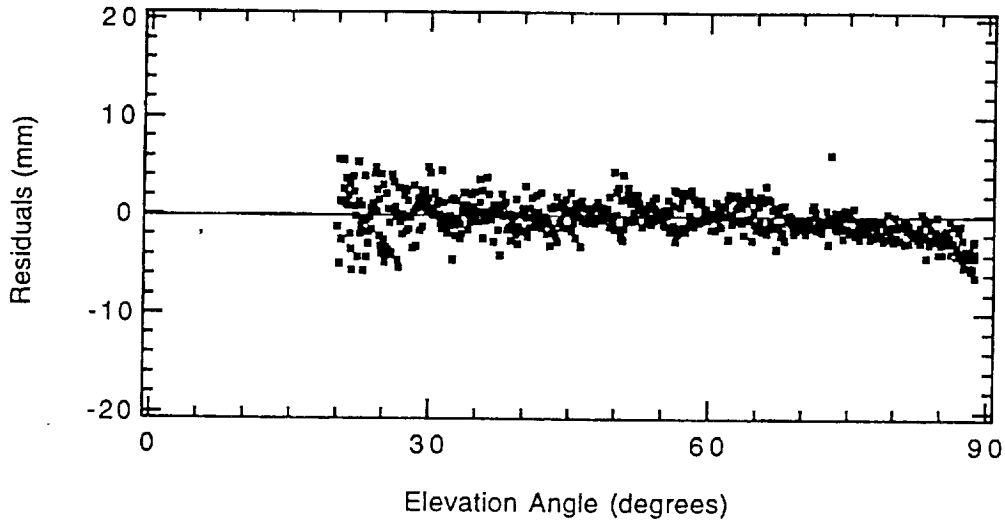
Residuals (mm)
20
10
0
-10
-20
0
30
60
90
Elevation Angle (degrees)

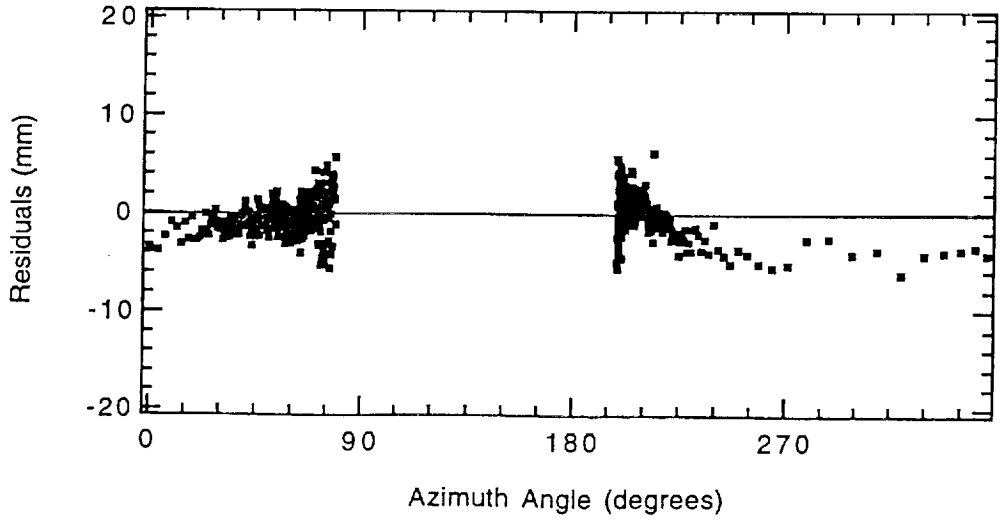
Residuals (mm)
20
10
0
-10
-20
0
90
180
270
Azimuth Angle (degrees)

Fig 9

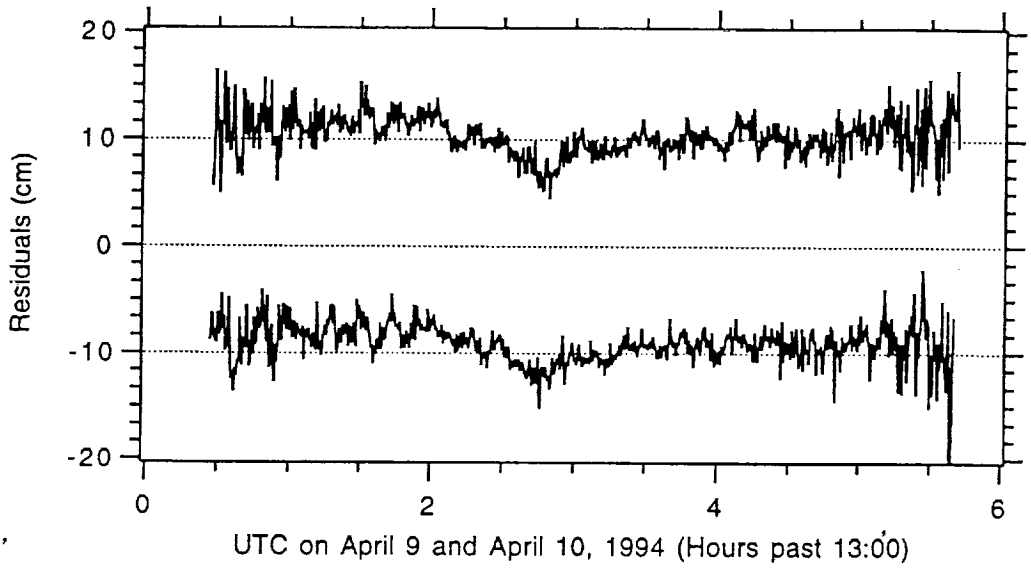
20
10
0
-10
-20
Residuals (cm)
0
2
4
6
UTC on April 9 and April 10, 1994 (Hours past 13:00)

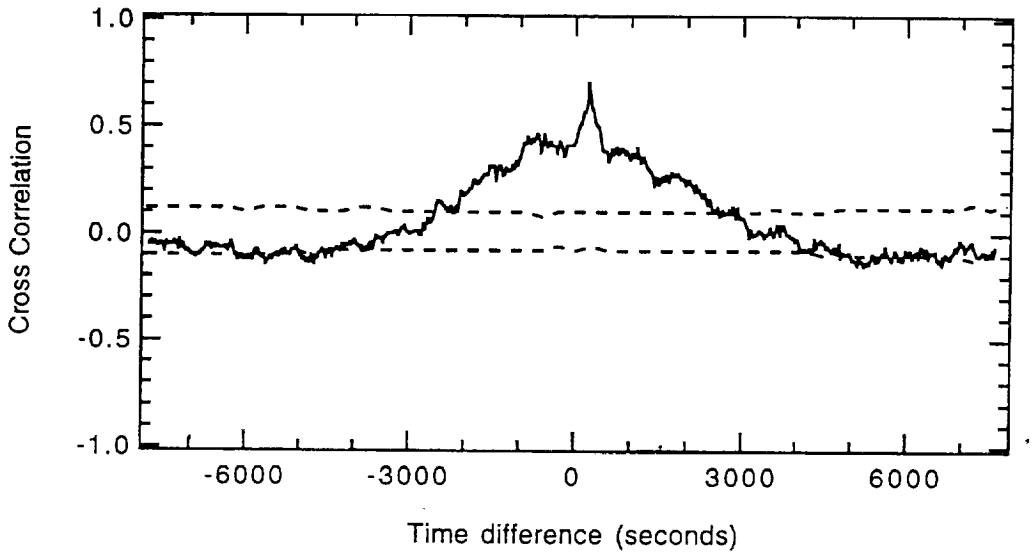
1.0
0.5
0.0
-0.5
-1.0
Cross Correlation
-6000
-3000
0
3000
6000
Time difference (seconds)

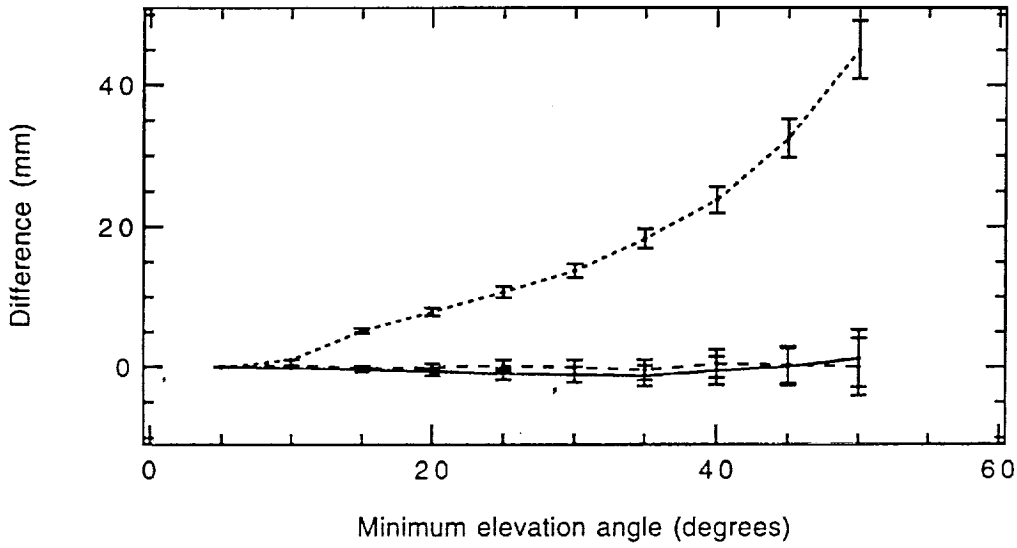
Difference (mm)
40
20
0
0
20
40
60
Minimum elevation angle (degrees)

Fig 12

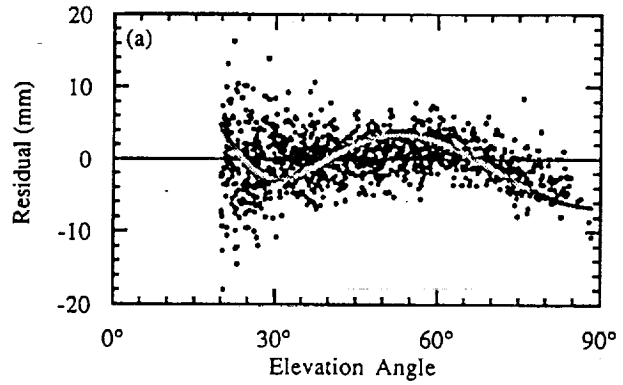
(a)
20
10
0
-10
-20
Residual (mm)
0°
30°
60°
90°
Elevation Angle

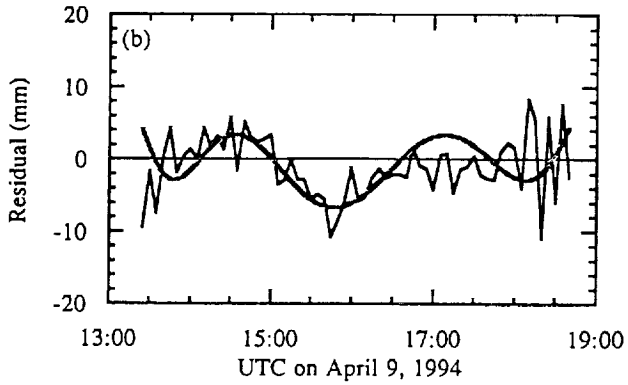
(b)
20
10
0
-10
-20
Residual (mm)
13:00
15:00
17:00
19:00
UTC on April 9, 1994

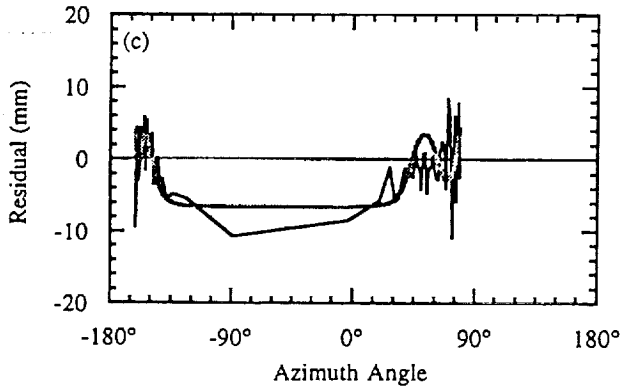
(c)
20
10
0
-10
-20
Residual (mm)
-180°
-90°
0°
90°
180°
Azimuth Angle

Fig 13

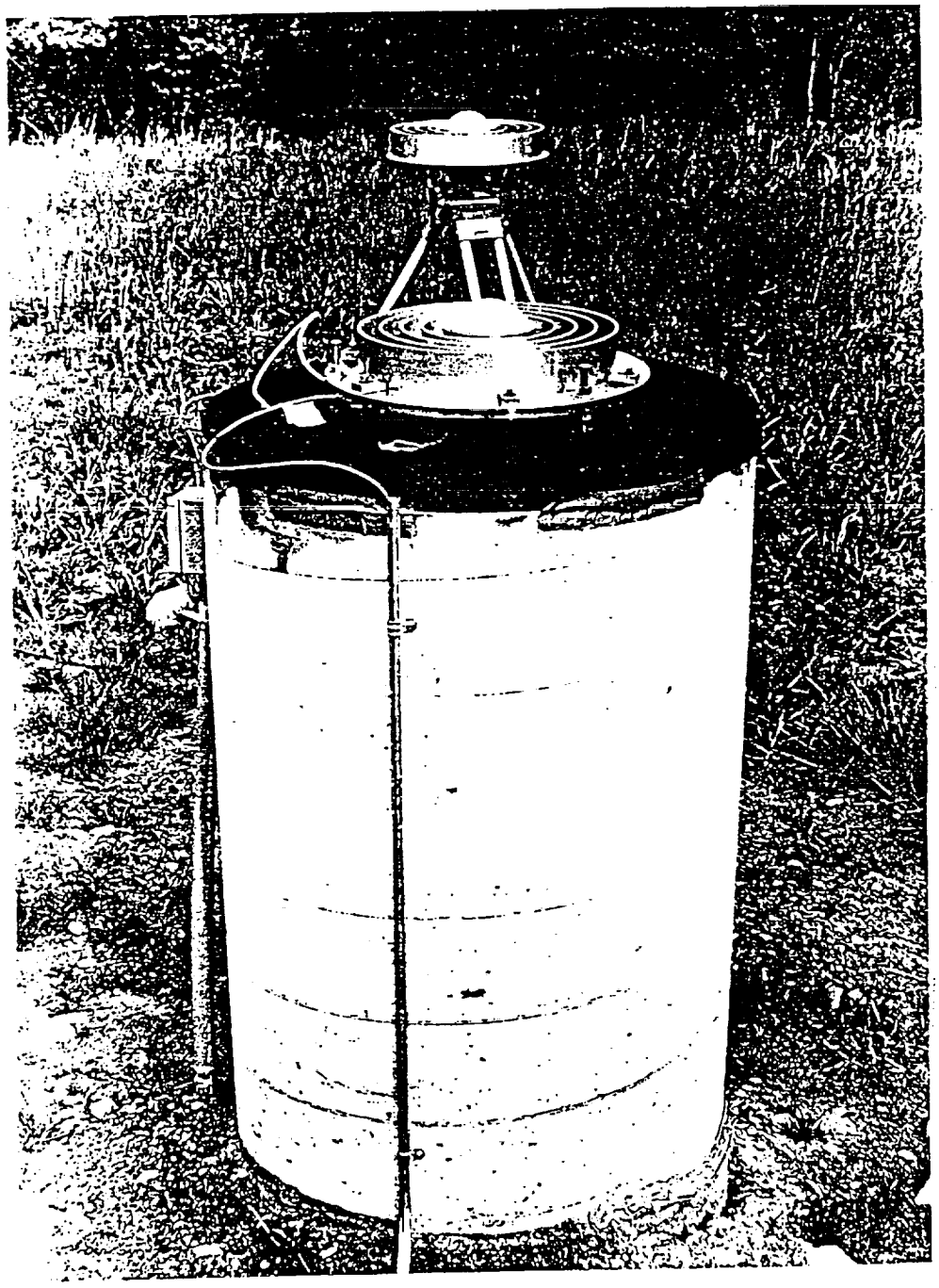

Fig 15

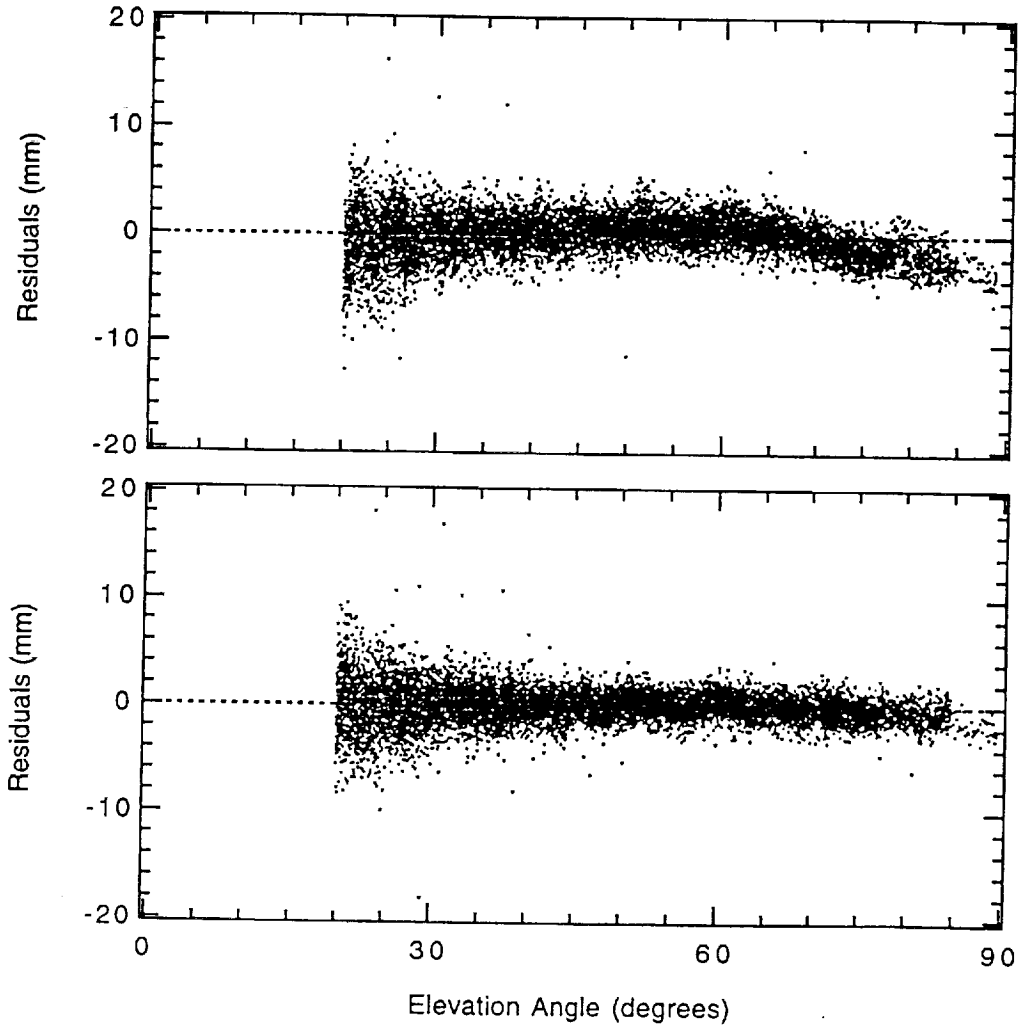
20
10
0
-10
-20
Residuals (mm)
20
10
0
-10
-20
Residuals (mm)
0
30
60
90
Elevation Angle (degrees)

Fig 15

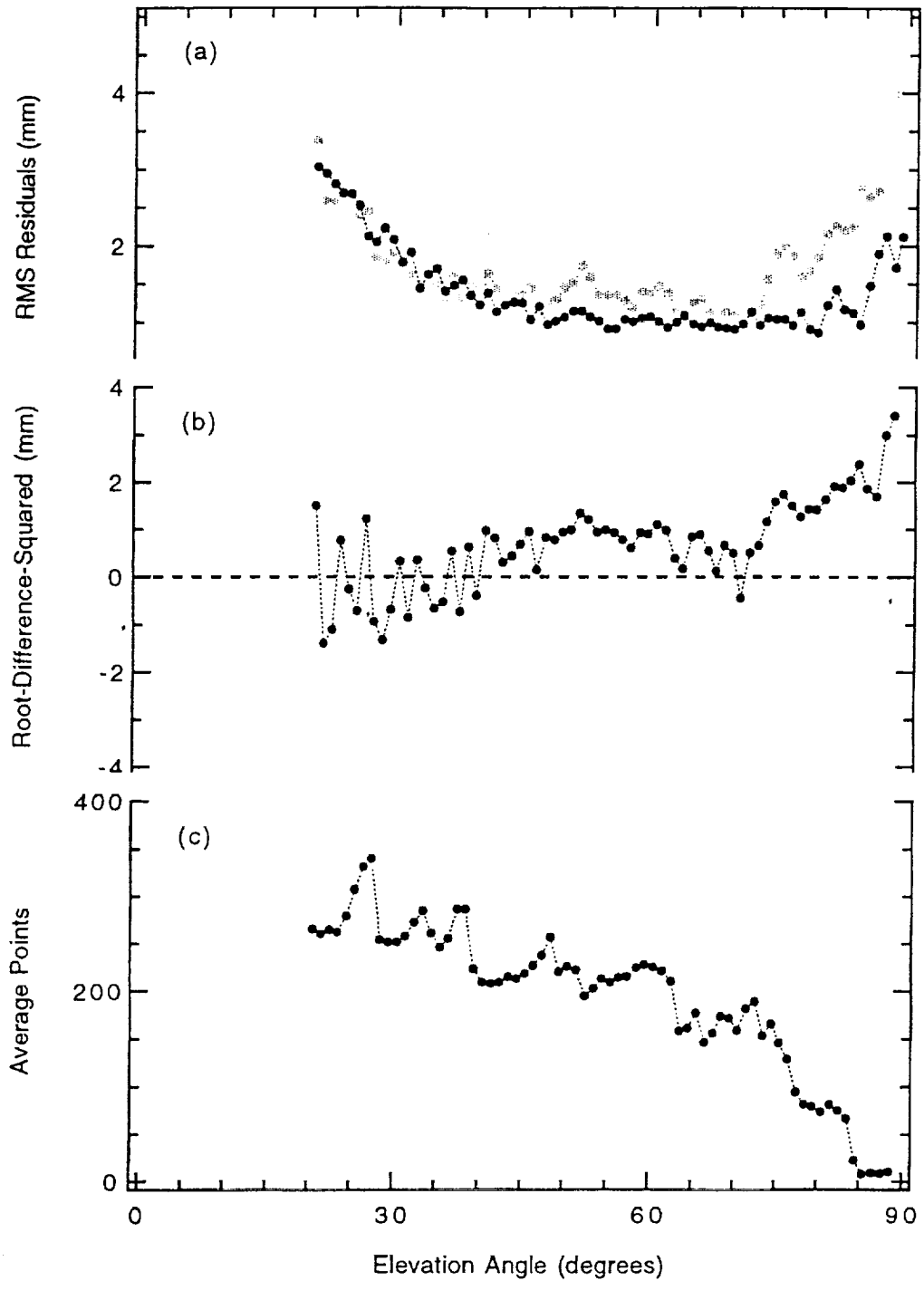
(a)
RMS Residuals (mm)
4
2
(b)
Root-Difference-Squared (mm)
4
2
0
-2
-4
(c)
Average Points
400
200
0
0
30
60
90
Elevation Angle (degrees)

Fig 16

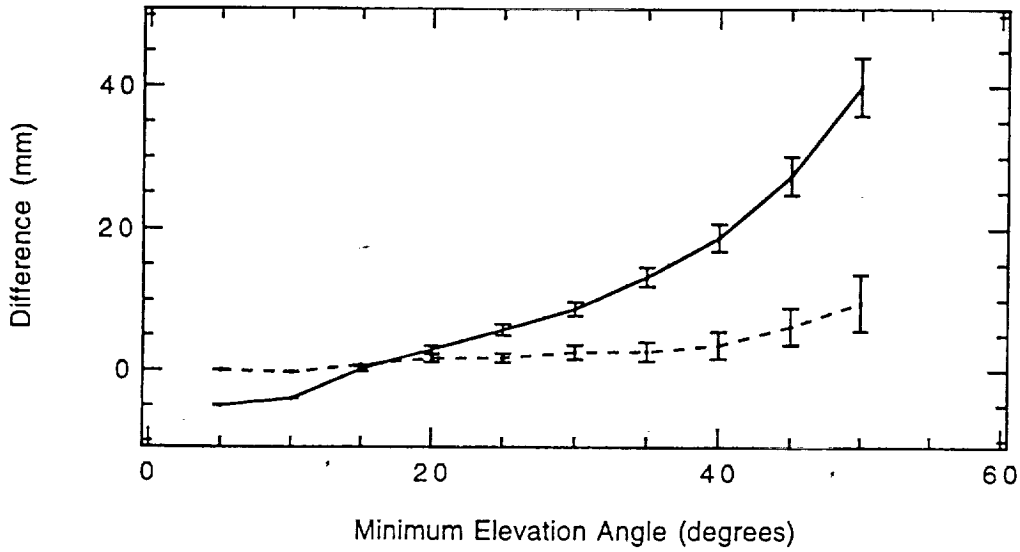
Difference (mm)
40
20
0
0
20
40
60
Minimum Elevation Angle (degrees)

Fig 17